J Solid State Electrochem (2011) 15:985–1006
DOI 10.1007/s10008-010-1214-6

REVIEW

Deposition and characterisation of epitaxial oxide thin films for SOFCs

José Santiso · Mónica Burriel

Received: 21 September 2010 / Revised: 1 October 2010 / Accepted: 4 October 2010 / Published online: 24 October 2010

Abstract This paper reviews the recent advances in the use of thin films, mostly epitaxial, for fundamental studies of materials for solid oxide fuel cell (SOFC) applications. These studies include the influence of film microstructure, crystal orientation and strain in oxide ionic conducting materials used as electrolytes, such as fluorites, and in mixed ionic and electronic conducting materials used as electrodes, typically oxides with perovskite or perovskite-related layered structures. The recent effort towards the enhancement of the electrochemical performance of SOFC materials through the deposition of artificial film hetero-structures is also presented. These thin films have been engineered at a nanoscale level, such as the case of epitaxial multilayers or nanocomposite cermet materials. The recent progress in the implementation of thin films in SOFC devices is also reported.

Keywords Thin films · Solid oxide fuel cells (SOFC) · Epitaxial · Ionic conducting materials · Mixed conducting materials (MIEC) · Anisotropy · Cathode · Anode · Electrolyte · Multilayers · μSOFCs · PLD

J. Santiso (✉)
Centro de Investigación en Nanociencia y Nanotecnología,
CIN2 (CSIC/ICN),
Campus UAB, Bellaterra,
08193 Barcelona, Spain
e-mail: jsantiso@cin2.es

M. Burriel
Department of Materials, Imperial College London,
Exhibition Road,
London SW7 2AZ, UK

Introduction

Present research in materials for solid oxide fuel cell (SOFC) technology is mainly focused in decreasing the operating temperature of the fuel cell to the intermediate range (500–700 °C) in order to avoid the materials' thermomechanical degradation of the fuel cell components at higher operation temperatures (typically above 800 °C), which reduces the devices' lifetime and obliges the use of expensive high-temperature-resistant materials, increasing the overall cost of the cells. This is particularly important when dealing with cell stacks where ceramic interconnect elements based on expensive chromium oxides or chromium-based metal alloys are required. The reduction of the working temperature diminishes the degradation and the interdiffusion between the different materials in the cell. Besides, it reduces the mechanical failure induced by the differences in thermal expansion coefficient of the different materials. However, it has a direct implication in slowing down the kinetics of the different thermally activated processes taking place in the cell, mainly oxygen surface exchange at the electrodes and bulk oxide ionic transport across the electrolyte. For this reason, it is necessary to explore new materials with increased performance or to develop new strategies with existing materials for enhancing their conductance, which may include reducing the thickness of the electrode/electrolyte current path or modifying the materials microstructure to induce fast transport paths along non-blocking interfaces or other type of defects. These different approaches will be discussed in detail in the following paragraphs.

In the last decades, there has been a progressive tendency towards the use of thinner SOFC elements, particularly in the case of the electrolyte, which is one of the main causes limiting the oxide ionic transport in the

cell. In order to attain large power densities of the order of 0.1–1 W/cm^2 at intermediate working temperatures, the implementation of methods to deposit thick films (from a few hundreds of microns down to almost 1 μm) has been required and progressively more complex thin-film technologies for thicknesses below 1 μm have been developed. Most current applications require large power generation, in the kilowatt and megawatt regime, making necessary the fabrication of SOFC devices with large effective surfaces, mostly stacks. However, there is a niche for lightweight low-power sources for devices requiring below 10 W, particularly for portable devices and remote small-scale sensors/actuators. For these devices, the fabrication of micro-solid oxide fuel cells (μSOFCs), based on similar thin-film technologies as those developed for microelectronics industry, is an emerging and highly active field of research that is attracting greater attention [1].

For the knowledge of the fundamental physicochemical properties of the materials involved in SOFC devices, it is essential to be able to separate those that are intrinsic to the materials from those that are caused by their microstructure or the presence of secondary phases or interfaces. This is sometimes a difficult task to achieve when dealing with polycrystalline ceramic samples and particularly if the films are prepared from methods that use additives and high-temperature post-treatments, in which there are too many parameters to control. For this reason, from a fundamental point of view, it is advisable to use test samples with more controlled microstructures and composition. This is generally the case of single crystals or thin films deposited from the vapour phase, either by physical or chemical methods. In most of the cases, it might be extremely difficult to grow single crystals of complex oxide materials, and the best approximation to obtain a material with similar properties to the single crystal is to grow epitaxial films.

In the following, we will only refer to oxide conducting materials for SOFCs, although in the last years there has been an increasing interest in oxide materials with protonic conductivity. The characteristics of those materials are sometimes very similar to those of oxide ionic conducting materials; for a comprehensive review on that topic, the reader is referred to [2].

Epitaxial thin films for SOFCs

The term *epitaxy* derives from the Greek roots *epi*, meaning 'upon', and *taxis*, meaning 'arrangement, order'. Epitaxial growth refers to the continuation of the alignment of crystallographic atom positions in the single-crystal substrate into the single crystal film. More precisely, an interface between film and substrate crystals is *epitaxial* if atoms of the substrate material at the interface occupy natural lattice positions of the film material and vice versa [3]. Epitaxial films constitute an ideal frame for fundamental studies of the intrinsic material transport properties, offering, in the case of anisotropic materials, the possibility of independently measuring each direction's component. In addition, they can also be used as models to study the properties variation by using substrate-induced strain.

Finally, this type of growth enables the deposition of artificial film heterostructures engineered at a nanoscale level, which can enhance the electrochemical performance of SOFC materials, as will be discussed in the next sections.

Deposition techniques for epitaxial thin films

Currently used techniques for the deposition of highly controlled epitaxial thin oxide films and multilayers include molecular beam epitaxy (MBE), pulsed laser deposition (PLD) [4], RF magnetron sputtering, e-beam evaporation, metal-organic chemical vapour deposition (MOCVD) and atomic layer deposition (ALD). It is not the aim of this work to describe in detail those techniques; an extended review on the different techniques can be found in [5].

During the deposition process, usually, the required material (or combination of materials) is supplied from a source (or different sources) and transported in vapour phase towards the substrate surface, where the deposition and further film growth take place. There are two main important requirements in order to obtain an epitaxial growth. First, the material has to be supplied to the substrate surface in atomic, molecular or ionic form with species consisting of a very few atoms, in order to guarantee a proper mixing of the constituents at a nanometre scale. This is easily achieved in vapour form produced from a solid source by thermal, arc, laser, e-beam evaporation or sputtering or from a liquid source by evaporation (pulsed-injection MOCVD) or spraying (spray pyrolysis). Then, the species are transported, mixed if necessary and adsorbed onto the surface by a physical or a chemical process. Second, there should be sufficient energy of the adsorbed species to diffuse along the surface in order to reach the equilibrium sites to form the crystal. In some cases, the incorporation into the solid is also mediated by a chemical reaction between the elements to form a different compound (CVD, ALD and reactive evaporation). Normally, the required energy is supplied thermally either by heating the substrates at temperatures from 400 to 1,000 °C or by activated processes making use of plasma sources, as in plasma-enhanced MOCVD, pulsed laser deposition or sputtering, techniques that allow the use of lower substrate temperatures while maintaining a high degree of crystallinity.

If the surface diffusion during the film deposition is limited by insufficient energy or by a too fast material supply rate, deposits with a low degree of crystallinity,

amorphous or even porous films, are obtained. Still, in those cases, in order to activate the bulk diffusion, a post-annealing process at high enough temperatures (usually above the deposition temperature) may result in the rearrangement of the elements in the solid and may produce highly crystalline films.

One of the most interesting characteristics of vapour-deposited films is that the film growth generally takes place at conditions far from thermodynamic equilibrium, thus allowing the growth of metastable materials with unique microstructure, which may show different properties from the bulk materials. One example of these metastable structures is the material obtained in multilayer form by sequential deposition of two different compounds. In the extreme case of superlattices, by combining sequential growth of two different structures at elementary level (with control over atomic layer or unit cell thickness and perfectly flat interfaces), it is possible to obtain artificial structures with a new periodicity and, in some cases, to induce novel physical properties.

Substrate requirements

In order to grow an epitaxial film of a certain material with its atoms perfectly arranged on top of the atoms of the selected substrate, the first requirement is to have a good crystallographic lattice match between film and substrate for the chosen orientation (generally below 1% mismatch) [6]. If the film and substrate lattice parameters are exactly (or virtually) the same, the film is expected to grow unstressed, and therefore, the intrinsic material properties of the film can be measured. In this case, the film's properties would be equivalent to those of a single crystal of the same composition (both the preparation and the characterisation of thin films being much simpler and unproblematic than those of single crystals). Alternatively, the choice of a substrate with a certain mismatch, i.e. with cell parameters either somewhat larger or smaller than those of the film, results in films grown under tensile or compressive strain, respectively. Figure 1 illustrates as example a perovskite epitaxial thin film of LSCF (a=3.8753, b=3.8769, and c=3.8827 Å) grown on $SrTiO_3$ (a=3.905 Å) under tensile strain (Fig. 1a) and the same film grown under compressive strain (Fig. 1b) on a different substrate ($NdGaO_3$, basal a–b plane parameter a_p=3.866 Å). The implications of the epitaxial strain in the materials' properties will be explained in the subsequent section. Finally, if the lattice parameters of the film and the substrate differ highly in all possible matching crystallographic orientations, it will not be possible to grow an epitaxial film, and the result will be either a preferentially oriented or a randomly oriented film.

Furthermore, it has been proven that, by controlling the termination plane of the substrate surface structure at an atomic scale, the chemical composition of the terminating layer can be varied. Kumigashira et al. [7] reported on the fabrication of $La_{0.6}Sr_{0.4}MnO_3$ (LSM) thin films in which the terminating layer was changed from B to A site by inserting one atomic layer of SrO between the LSM film and a TiO_2-terminated $SrTiO_3$ (001) substrate. This is expected to have an influence in the surface exchange properties of the material and might be crucial for the film growth of heterostructures with sharp interfaces [8, 9].

The second substrate requirement, in order to obtain a thermally stable film, is to have similar thermal expansion coefficients between film and substrate. Otherwise, when temperature changes take place (first from deposition temperature to room temperature and afterwards by subsequent cycling between room and working temperatures), cracks could appear on the film's surface, as well as delamination or corrugation problems.

In addition, for a good chemical stability between film and substrate, the materials should be chemically inert at the film–substrate interface under the specific experimental conditions. Alternatively, if this condition is not fulfilled or if the mismatch with the substrate is too large, it is possible to use buffer interlayers of chemically inert materials, in which cell parameters should also be in good match with the film and the substrate.

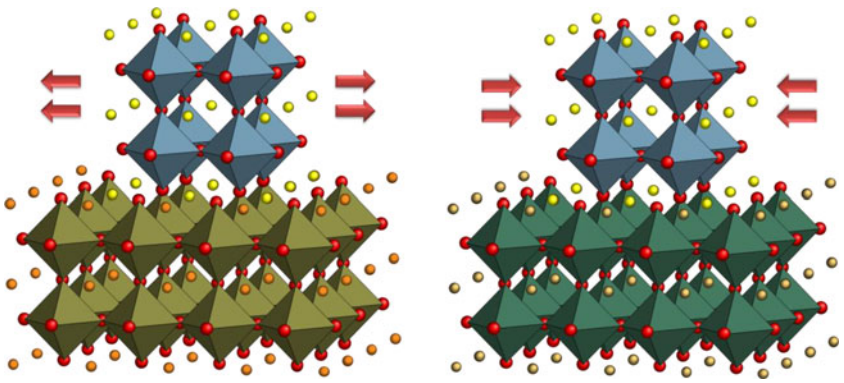

Fig. 1 Scheme of a perovskite epitaxial thin film of LSCF (a=3.8753, b=3.8769, c=3.8827 Å) grown on $SrTiO_3$ (a=3.905 Å) under tensile strain (**a**) and on $NdGaO_3$ (basal a–b plane parameter a_p=3.866 Å) under compressive strain (**b**)

Finally, depending on the thin films' further use and characterisation, additional properties can be required. One should always confirm that there is no interference or interaction with the substrate's properties. For example, if the intention is to selectively measure the electronic transport properties of the thin film, the substrate should be insulating, whereas in the case of characterising the electrochemical properties of the thin film when working as an electrode, the substrate should be oxygen conducting to act as electrolyte.

Epitaxial strain

In the case a certain film–substrate mismatch is present, different mechanisms, either elastic structural changes or plastic deformations mediated by the generation of defects, permit partial or total strain accommodation. These structural and compositional changes in the materials can induce, for example, variations in the electronic and ionic transport of the films. For instance, epitaxial films of the perovskite $La_{0.8}Sr_{0.2}CoO_3$ (LSC) deposited on yttria-stabilised zirconia (YSZ) single crystals by PLD showed different electrode properties depending on the orientations. The LSC films on the YSZ (100) and (111) substrates showed the (110) orientation with different twin structures, while those on the YSZ (110) had (100) and (112) orientations [10]. Ideally, one could tune the electrolyte or electrode properties by using substrates with different cell parameters in order to optimise the performance of the SOFC. When studying strain-induced effects occurring at intermediate or high operation temperatures, one should always take into account the thermal expansion coefficients of both substrate and film, as the induced stress could be consequently reduced or enhanced.

There are some limitations for the deposition of strained films which are related to the elastic properties of the film material. The thicker the film, the higher is the elastic energy accumulated, proportional to the volume of the material. Above a certain threshold thickness, the material is not capable of maintaining its structure and tends to release energy either by generating defects (i.e. misfit dislocations, domains with different orientations and phase segregation) or by modifying its surface morphology (surface roughening and island formation). Those effects have to be taken into account and could be of interest for the enhancement of the materials performance, such as in the case of ionic transport along defects, as discussed in 'Electronic transport'.

Transport anisotropy

In the case of anisotropic materials, such as layered mixed ionic–electronic conducting (MIEC) cathodes, it is particularly interesting to be able to grow epitaxial films of different orientations, which can be done by either using substrates with different cell parameters or by varying the deposition conditions of the thin film. This opens the possibility of evaluating anisotropic properties in different directions and of maximising the properties of a particular SOFC component (either the electrolyte or the electrode) by growing the material in a particular crystallographic direction. Figure 2 exemplifies the case of a double-perovskite material, $GdBaCo_2O_{5+x}$, grown on a $SrTiO_3$ substrate in three different directions: *a*-, *b*- and *c*-oriented. As this material is anisotropic, as will be discussed in detail in 'Measurements', the properties of the epitaxial thin film could be different for each of these three cases. This anisotropy has been proven by Shinomori et al. who grew *a*- and *c*-axis-oriented epitaxial thin films of layered nickelate $La_{2-x}Sr_xNiO_4$ on $LaSrAlO_4$ (100) and $(LaAlO_3)_{0.3}(SrAl_{0.5}Ta_{0.5}O_3)_{0.7}$ (001) substrates (LSAT), respectively [11]. In the *a*-axis-oriented films, the resistivity and the optical spectra showed large anisotropy between the *b* and c axes, indicating the quasi-two-dimensional nature of the electronic structure in $La_{2-x}Sr_xNiO_4$. Another example is the low-temperature anisotropic oxygen diffusion reported by *Inoue* et al. in perovskite structure iron oxides [12]. Deposition on STO and LSAT yielded pseudo-tetragonal $CaFeO_{2.5}$ epitaxially grown thin films oriented on the c_p(*b*)-axis and $CaFeO_{2.5}$ oriented on the a_p-axis on LAO and LSAO substrates. The structural changes when single-crystalline $CaFeO_{2.5}$ films were changed into $CaFeO_2$ by low-temperature reductions with CaH_2 were observed, implying that oxygen diffusion in the brownmillerite structure is highly anisotropic.

The methodology for the characterisation of anisotropic ionic/electronic properties is described in the next section.

Characterisation of ionic/electronic properties

In this section, we will focus on the characterisation of the most relevant properties for thin films for SOFC: charge transport, diffusion properties and surface exchange rates. For the description of more general techniques commonly used for chemical composition, structure, orientation and surface morphology characterisation, the reader is referred to [5].

Electronic transport

Electric conductivity measurements on thin films are normally performed either by using DC or AC techniques. Here, we outline the main configurations as well as the particular limitations and problems encountered when working with thin films. A more comprehensive description about these types of measurements can be found in a recent review by Guo [13].

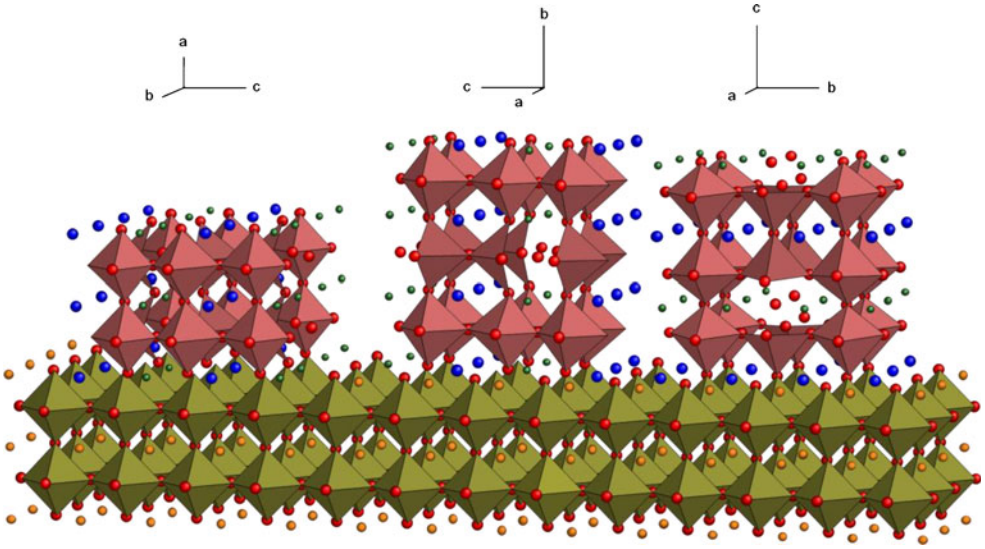

Fig. 2 Scheme of $GdBaCo_2O_{5+x}$ (a=3.881, b=7.829, c=7.542 Å [185]) double-perovskite epitaxial thin films grown on a $SrTiO_3$ substrate with different orientations: a-axis (**a**), b-axis (**b**) and c-axis (**c**)

DC measurements

DC measurements give information about the overall charge transport process and very often include a combination of the different mechanisms taking place in the film. Longitudinal measurements can be performed in a very simple two-point contact configuration (illustrated in Fig. 3a), by defining two parallel metal contacts (typically Ag, Au or Pt contacts evaporated through shadow masks or directly painted with metal colloids) on the surface of the film, forcing the current to flow along the film plane. Note that, in the four schemes in Fig. 3, for a better visualisation, the thin-film thickness L has been represented much larger than its actual dimensions; in reality, the lateral dimensions and the distances of the electrodes are much larger than L. For the transverse measurements, it is necessary to define metallic contacts on the top and on the bottom of the film, as shown in Fig. 3b. Since the films are supported on a substrate, for the bottom contact, either the substrate is conducting enough (Nb-substituted $SrTiO_3$ single crystals are very often used providing low resistance, particularly at low temperatures) or a thin metallic bottom contact (such as Pt, $SrRuO_3$ and $LaNiO_3$) is deposited between the film and the substrate. For the growth of epitaxial films, in order to guarantee the structure coherence of the whole heterostructure, the bottom metallic electrode should also be epitaxial, offering a good film–substrate match.

There are some restrictions to the use of DC measurements in thin films:

1. There should be no substantial charge accumulation in none of the interfaces within the material system or the contacts' surface, preventing the building up of a capacitance. In the longitudinal configuration (Fig. 3a),

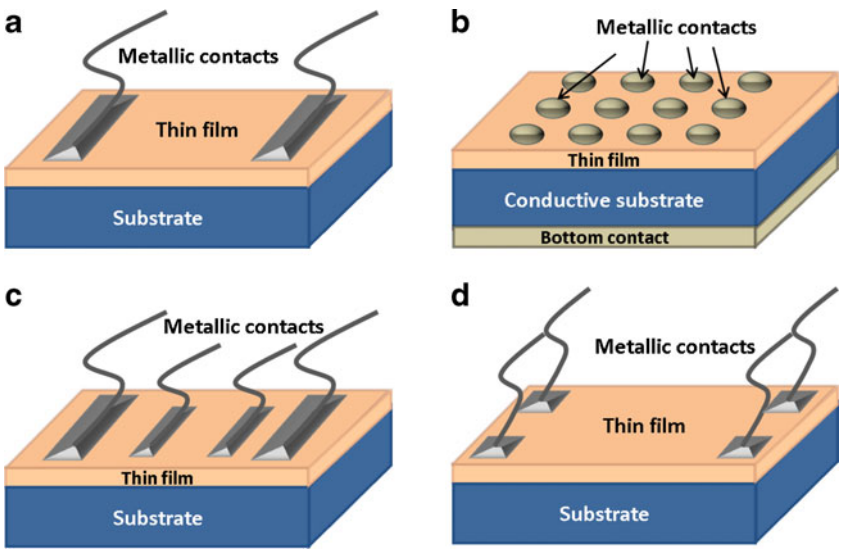

Fig. 3 Different electronic transport measurements configurations: longitudinal two-point contact configuration (**a**); transversal configuration (**b**); longitudinal four-point contact configuration with parallel contacts (**c**); and longitudinal four-point contacts with van der Pauw rectangular configuration (**d**). Please note that the thickness of the thin film (L) is grossly exaggerated when compared with the thickness of the substrate; in reality, the lateral dimensions and the distances of the electrodes are much larger than L

as the film thickness (L) is orders of magnitude smaller than the contact length and distance, the geometrical factor makes the capacitance negligible in comparison to other stray capacitances in the experimental setup. However, in the case of transverse measurements (Fig. 3b), the capacitances could become important, particularly in the case of electronic transport in semiconducting oxide materials, and even larger in the case of electronic insulating electrolyte materials, as those typically used in SOFCs. In those cases, AC measurements are normally performed.

2. The conductance of the film material should be large enough in comparison to any other conductance in the transport path. In highly conducting materials, the contact resistance might be comparable to the film resistance. In those cases, a proper four-point contact, either with parallel contacts (Fig. 3c) or in a rectangular van der Pauw configuration (Fig. 3d), enables the elimination of the contribution of the resistance generated from the voltage measurement at the current contacts. On the other hand, in the case of highly resistive materials and particularly for very thin layers, the film resistance might become comparable to the substrate resistance. A proper choice of the substrate material and of the measurement conditions (temperature and gas atmosphere) is required to guarantee a homogeneous current flow through the film section.
3. In most of the materials used in SOFC, there are several types of charge carriers involved (electrons, holes and ions) in the transport phenomena. Particularly, in mixed ionic–electronic conductors used in SOFC electrodes, the ionic conductivity can become comparable to the electronic conductivity (*n*-type or *p*-type component). Still, in those cases, under certain temperature and oxygen partial pressure conditions, the total conductivity can be associated to the majority carriers. However, no information is obtained from the minority carriers, which very often play an important role in the electrochemical processes. Indirect information can be extracted from the extrapolation of the conductances to the regions where those carriers become predominant. Alternatively, the use of proper materials as electrodes may allow the selective blocking of the majority carriers, in order to reach a steady state in which the conductivity is only related to the minority carriers. For instance, pure oxide ionic conducting YSZ electrodes will block the electronic conductivity, while dense Pt electrodes are considered oxide ion blocking. On the other hand, Ag electrodes are considered reversible for electronic and oxygen transport. These are the 'Hebb–Wagner' methods, described in detail in [14].

Impedance spectroscopy (AC measurements)

AC measurements are generally performed on semiconductors and insulating materials when the samples present charge diffusion with characteristic non-negligible time responses and in processes in which there is a coexistence of several charge transport phenomena, as in SOFC, i.e. oxide ionic transport within the electrolyte grains or across grain boundaries, electronic transport in the electrodes, oxygen incorporation from the gas phase by reduction on the cathode or fuel oxidation at the anode. Each of these processes shows a characteristic time constant τ (related to its equivalent circuit, mostly a combination of a resistance R and a capacitance C in parallel, so $\tau=RC$).The frequency response analysis of the impedance allows, in some cases, differentiation between those processes. Often, the measurements are limited by a high impedance value in a particular frequency range above the instrument input impedance. A proper patterning of the film geometry, either by defining a long and thin meander path (thus increasing the film resistance), by using interdigitated electrodes (reducing the film resistance and increasing its capacitance) or by using extremely small point contacts (increasing the film resistance and reducing its capacitance in transverse measurements), allows adjustment of the RC product to the measuring setup. Impedance analysis can become a quite complex task, and the information extracted from the raw data is very often dependent on the model used for the equivalent circuit associated to the system. For a more general description of the impedance analysis for SOFC materials, the reader is referred to [15].

Steady values of the total electric conductivity at different temperatures and pO_2 give information about the main carriers involved and about the defect equilibria associated to a particular material. From this information, it is often possible to extract some characteristic intrinsic properties of the material, such as the activation energies for thermally activated charge diffusion processes, the apparent gap energy (in semiconductors) and the reduction and oxidation enthalpies [16–18]. However, it is still difficult to separate the convolution between carrier density variations from the mobility of the carriers. In bulk materials, it is often possible to separate both conductivity components either by performing Hall measurements or by measuring thermoelectric power [19–21]. Hall voltage induced by an applied magnetic field is proportional to the carrier mobility. Therefore, in materials with fairly small carrier mobility, such as band insulators, ionic conductors and even in electronic polaron semiconductors, the characterisation by this method is hampered by the small voltages generated. Thermoelectric power measurements are based on the characterisation of the small voltages generated by a temperature gradient induced in the sample between two

electrodes. Unfortunately, in thin samples, the small dimensions, along with the presence of a substrate material, make it extremely difficult to extract any information from this type of measurements, and so far, there are no reports in the literature for thin films of typical SOFC materials.

Oxygen diffusion and surface exchange properties

Knowledge of the relevant transport parameters of the solid oxide materials involved is of fundamental importance in the development of SOFC devices. A variety of techniques have been developed, by which it is possible to determine, in addition to bulk transport coefficients, surface exchange constants. There are three fundamental experimental techniques usually applied to obtain transport coefficients: (1) the chemical experiment (electrical conductivity relaxation), in which the oxygen stoichiometry is changed; (2) the tracer experiment (isotope exchange depth profile method), in which the tracer distribution is changed; and (3) the electrical experiment (impedance spectroscopy) in which an outer electrical potential gradient is applied as from a driving force. It must be noticed that the three diffusion coefficients, D_{Chem}, D^* and D_{Q}, and three rate constants, k_{Chem}, k^* and k_{Q}, obtained from the three techniques, respectively, are intrinsically different and, as a general rule, cannot be directly compared [22].

Epitaxial films constitute ideal model materials to measure diffusion coefficients, as they typically are completely dense. Accordingly, in the case of the materials' characterisation, the oxygen transport will have no influence on non-kinetic issues, such as particle morphology and connectivity, porosity and tortuosity, typical in porous electrodes.

Electrical conductivity relaxation

Monitoring of the DC conductivity changes when exposing a sample to an oxygen partial pressure step variation in the surrounding atmosphere (Fig. 4) may provide information about the kinetics of the different processes taking place in the sample [23, 24]. These processes are mainly the oxygen surface exchange with the atmosphere, either the in-take or out-take depending on the initial and final pO_2, and the oxygen bulk diffusion. When dealing with very thin samples, the time necessary for the oxygen to diffuse through the thickness of the film can be considered negligible in comparison to the time required for the oxygen surface exchange. Therefore, the conductivity changes mainly reflect the surface exchange processes and are generally adjusted by a single exponential time dependence (provided the pO_2 step change is small enough to associate a linear response to the conductivity change). The characteristic time is related to the surface exchange rate k for a given temperature and pO_2 range. The

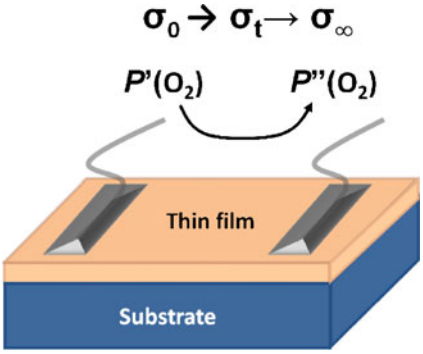

Fig. 4 Schematic of the ECR measurements of a thin film on a substrate. Please note that the thickness of the thin film (L) is grossly exaggerated when compared to the thickness of the substrate

limitations for this measurement are related to the rate at which the gas can be exchanged in the experimental setup in comparison to the surface exchange kinetics and are therefore often restricted to low temperatures. Alternatively, Tragut et al. [25] developed a method (conductivity relaxation in the frequency domain) that produces a modulation in the total gas pressure at varying frequencies by means of magnetic valves, which induces a periodic response in the conductivity of the sample. By monitoring the amplitude and the frequency response of the delayed signal, the authors are capable of extracting the surface exchange coefficient of the sample. This technique has been validated and used for thin films, obtaining values of the surface exchange coefficient up to 700 °C for epitaxial BSCF films [26].

Isotope exchange depth profile method

The oxygen isotope exchange technique consists of exchanging the ambient oxygen surrounding an oxide, which is usually an isotope mixture primarily made up of ^{16}O, with a gas enriched with ^{18}O (or ^{17}O). The specimen is usually pre-treated in the oxygen partial pressure and temperature of the exchange measurement itself in order to establish thermodynamic equilibrium and prevent effects of chemical diffusion within the sample bulk. The consequence of a difference between the tracer content of the gas and that of the solid phase is a tracer exchange in the solid. The total oxygen content ($^{16}O + {}^{18}O$) of the oxide remains constant during the exchange process, that is, the chemical composition is not altered. And so, this tracer diffusion is in fact a counterdiffusion of the two oxygen isotopes [27]. Data on these coefficients can be obtained from isotope exchange depth profiling by secondary ion mass spectroscopy after partial isotope exchange has taken place at the desired temperature and oxygen pressure. The tracer diffusion coefficient and the surface exchange coefficient are obtained by curve fitting of the measured profile to the appropriate equation, which is deduced from the solution to

Fick's second law with the appropriate initial and boundary conditions.

The development and validation of a new methodology for the determination of anisotropic tracer diffusion and surface exchange coefficients for epitaxial thin films by Burriel et al. [28] opened up the possibility of measuring a wide range of anisotropic materials, thin films and multilayers. The sample configuration and an outline of the ^{18}O diffusion profiles for the traverse and longitudinal oxygen tracer transport measurements are shown in Fig. 5. To measure the diffusion along the traverse direction, the oxygen concentration profiles are analysed using the analytical solutions to the diffusion equation for a plane sheet model developed by Crank [29]. And to determine the oxygen transport along the longitudinal direction in the plane of the film, a dense and uniform thin film of a different material (such as Au) is required to protect the film surface and prevent oxygen exchange from the surface. A trench should then be defined in the surface of the protecting film penetrating down to the substrate. The lateral edge of the film is then opened to allow the exchange with the ^{18}O-enriched exchange gas phase and thus ensuring the diffusion of the ^{18}O species only along the longitudinal direction of the film. The longitudinal concentration profiles obtained are analysed using a semi-infinite plane solution of the diffusion equation [28, 29].

Impedance spectroscopy

Electrochemical impedance spectroscopy is frequently used to determine the diffusion, kinetic and thermodynamic properties associated with oxygen transport in mixed conducting nonstoichiometric oxides. This technique, as has already been mentioned in 'Substrate requirements', allows independent measurement of the various component impedances if a satisfactory model for deconvoluting the relevant time constants can be developed. First, the distinctive features observed in the impedance spectra have to be assigned to the contributions from the ionic conduction of the electrolyte, oxide ion transfer across the electrode/electrolyte interface, and the oxygen exchange on the film surface. Then, an equivalent circuit model is used to analyse the impedance results, from which the surface chemical exchange coefficients can be derived. Several examples in which this technique has been used to extract the surface exchange coefficients of epitaxial thin films can be found in the literature [10, 30–32].

Recent developments in epitaxial SOFC materials

In the following paragraphs, we will show the recent developments achieved in the field of SOFC materials through the use of thin films, mainly in the form of epitaxial layers and heterostructures.

Thin-film electrolytes

One of the key points to increase the performance of solid oxide fuel cells has focused on the reduction of the electrolyte area-specific resistance. Obviously, the search for materials with improved ionic conductivity has been one of the most extended approaches. In this case, composition variations of existing well-known materials, such as ZrO_2 or CeO_2-based fluorites, by means of extrinsic substitution, and the development of new materials such as $LaGaO_3$-based perovskites, BiMeVOx aurivillius phases, apatites, etc., have been the subject of extended reviews [32–45]. But for real operation of SOFC devices, a more integral approach has to be adopted, taking into account other aspects, such as the chemical and thermomechanical compatibility with different types of electrodes. This aspect has been the subject of a major activity in the field [38, 46–61].

Other studies have pointed towards a geometrical approach which is to reduce the electrolyte thickness and to increase its surface area. While the second is still in its infancy, there have been some attempts to produce corrugated YSZ electrolyte films by means of lithographic

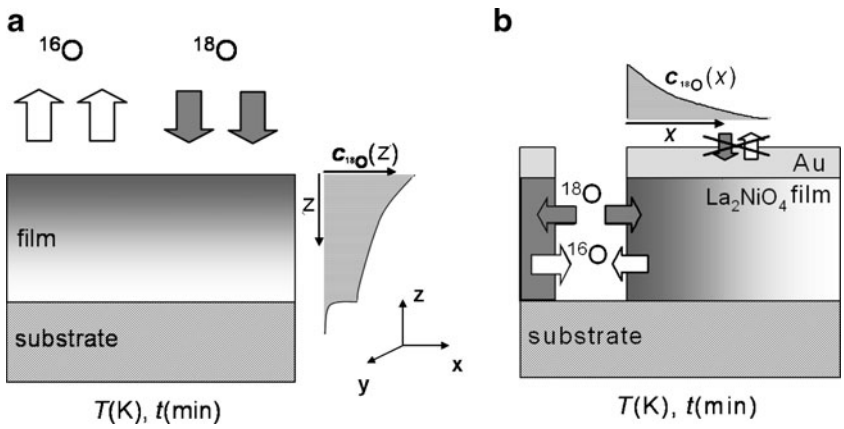

Fig. 5 Sample configuration for traverse **a** and longitudinal **b** oxygen tracer transport measurements. Reproduced with permission from [28] Royal Society of Chemistry © 2008

techniques [62], and some authors pointed out the possibility of using nanostructured templates, such as nanopillars or nanopores, to build up large specific area films. The reduction of the electrolyte thickness is an obvious way to increase the oxygen conductance, provided the material properties remain the same as in bulk material.

Given the multicomponent nature of the SOFC devices, once the oxide ion conductance at the electrolyte has reached a certain value, it might be that a further reduction of its thickness does not increase the performance of the cell, as there could be other steps in the overall process limiting the performance. Some authors have established a target value of area-specific resistance at about 0.15 Ω cm^2 [63] for the electrolyte, below which a further reduction is supposed not to be effective, provided standard values of the conductances of the rest of the components. This resistance could be attained for a film of 1 μm at temperatures of about 500 °C for YSZ and of 300 °C for Gd-doped ceria, assuming bulk conductivity values. However, considerable improvements can be expected for all the components, which make further increase in the electrolyte conductance of great interest, i.e. further thickness reduction towards the submicron scale.

Although there have been large improvements in some of the large-scale fabrication techniques generally used for depositing electrolyte films, such as tape casting or screen printing, they have encountered some limitations when trying to deposit thin films with homogeneous thicknesses below 1 μm. To overcome these limitations, there is an increasing usage of well-developed vapour-phase techniques, as those described in 'Deposition techniques for epitaxial thin films', which allow depositing films down to the nanometre scale with reasonable uniformity.

Nanocrystalline films: grain size effect

As is generally the case in polycrystalline materials, the charge transport and mass diffusion mechanisms across the material can be substantially different in the bulk of the grains and in the grain boundaries. Obviously, the smaller the grain size, the larger is the ratio between grain surface and bulk effects. In nanocrystalline samples, the interface effects may dominate the transport mechanisms, which could significantly modify the performance of the electrolyte material. In some cases, these interface effects have generated an enhancement of the ionic conductivity, as in YSZ epitaxial ultrathin films [64–67], as shown in Fig. 6. Kosacki et al. [66] reported two orders of magnitude enhancement in the film conductivity in epitaxial YSZ films of about 15-nm thickness deposited on MgO single-crystal substrates in comparison to bulk YSZ conductivity, along with a substantial reduction of the activation energy. A similar behaviour has also been reported for Gd-doped

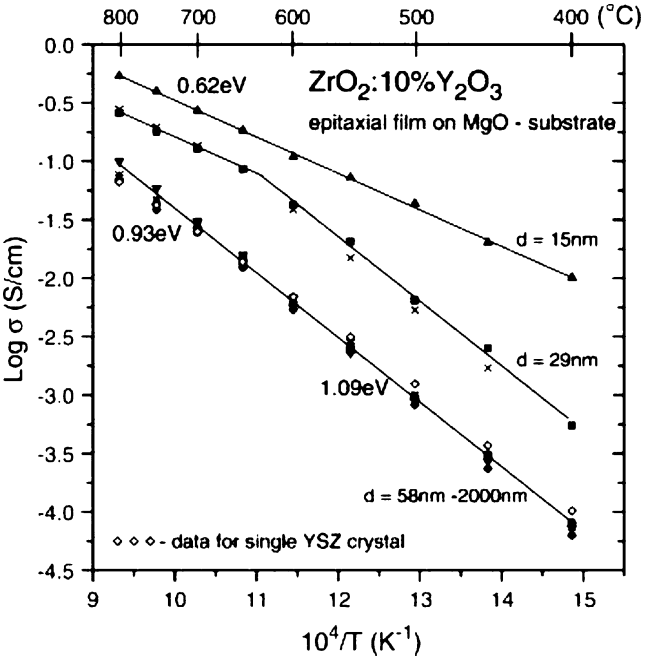

Fig. 6 Arrhenius plot of the conductivity for thin epitaxial films deposited on MgO single crystals. Reproduced with permission from [66]. Copyright 2005, Elsevier

ceria films, as shown in Fig. 7. However, the reduction of the film thickness might also induce the enhancement of the electronic conductivity in an electrolyte material, as in the case of nanocrystalline CeO_2 samples (also shown in Fig. 7) [16, 68–73], turning the material into a mixed ionic–electronic conductor.

Also, the grain boundary contribution to the electric transport may be different if the transport takes place along the interfaces or across them. In some cases, as in $SrTiO_3$ polycrystalline samples, the boundaries could have a blocking effect when the current is forced to flow across the boundaries [74], whereas the transport is enhanced parallel to the interfaces [75–77]. For the modelling of the whole charge transport mechanism, the combination of all contributions has to be taken into account, which is generally attained by using the 'brick-layer model' [77–81].

Nanocrystalline ceramic bulk materials are generally prepared from fine nanopowders, or via sol–gel processes. In those cases, to attain densification with a reasonable connectivity between grains, it is necessary to use severe high-temperature post-annealing steps of the order of 900–1,300 °C. This may produce certain instability of the metastable nanostructure, inducing grain growth [82, 83] or impurity segregation towards the grain boundaries (as in the typical case of Si impurities [84]) where they accumulate, producing clear blocking effects [74]. An important difference between nanocrystalline materials prepared from the standard solid-state reaction and materials deposited in the form of films by chemical or physical vapour deposition

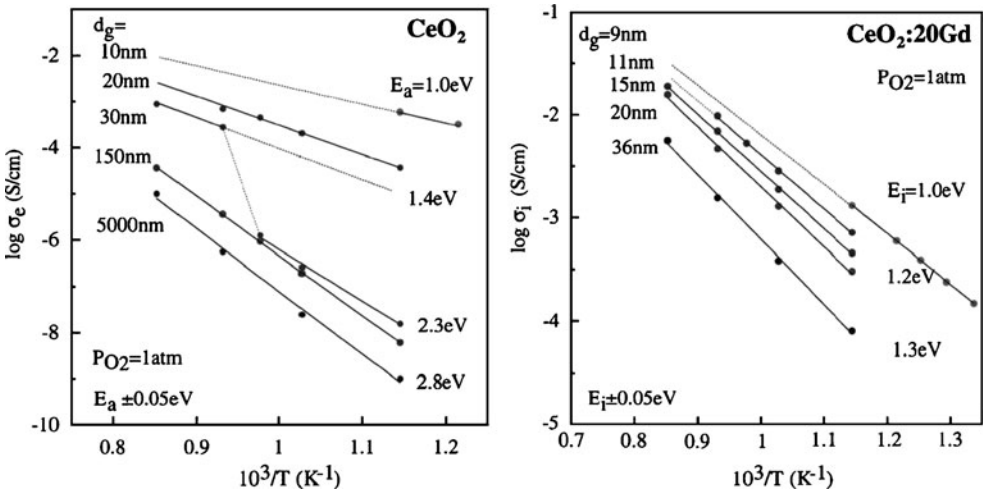

Fig. 7 Electronic conductivity for undoped CeO_2 (*left*) and ionic conductivity in Gd-doped CeO_2 (*right*) epitaxial thin films. Reproduced with permission from [72]. Copyright 2002, Elsevier

methods (MOCVD, ALD, e-beam evaporation, sputtering, pulsed laser deposition, etc.) is that from the vapour techniques it is possible to attain dense nanocrystalline microstructures at the deposition temperatures (generally well below 900 °C) without the need of further annealing steps, minimising therefore possible impurity segregation towards the grain boundaries. Besides, under some conditions, the use of vapour-deposited films induces the growth of preferentially oriented grains (in a columnar structure) which would generate certain anisotropy in the grain boundaries (aligned across the thickness of the film) and could have a favourable effect either directly in the charge transport mechanism or in the stabilisation of the nanostructured domains.

Combination of insulating–conducting materials/space charge effects

One of the most interesting approaches to enhance the ionic conductivity of electrolyte materials is based on the space charge effects generated at the interface between two different materials [13, 85]. At steady-state conditions, the different electrochemical potentials of the two materials in contact would balance by interdiffusion of charge carriers, thus modifying their equilibrium bulk charge concentration at the interface area with an extent of the order of the Debye length of the material [86]. The values could go from only a few nanometres to several tenths of nanometres, depending on the materials involved. If the composite material consists of nanometric-size crystal domains, then the space charge effects may prevail over the bulk behaviour. In some cases, as in BaF_2/CaF_2 multilayered heterostructures obtained by MBE [87], the concentration of the dominant ionic mobile species (fluoride ion interstitials and fluoride vacancies) could be largely depleted and increased, respectively, in the space charge region of BaF_2 material in contact with the CaF_2. This depletion would cause an inversion of the majority carriers, therefore inducing an increase in conductivity by several orders of magnitude along the direction parallel to the interface region, in proportion to the density of interfaces. It is also foreseen that a further reduction of the layer thickness would also make it possible to increase the charge transport across the layered structure [88]. A similar effect occurred on the ionic conductivity of lithium iodide–aluminium oxide composite solid electrolyte associated to the space charge regions [89].

This is possible in very diluted systems with high carrier mobility but low intrinsic concentration (as in BaF_2 where F^- is about 10^{17} cm^{-3} [13]). However, in oxide conducting materials such as disordered oxygen vacant fluorites or perovskites, in which the carrier concentrations are of the order of $10^{20–21}$ cm^{-3}(that is a few per cent per formula unit), a further increase in the density of vacancies is very limited (hardly reaching one order of magnitude). Besides, it would readily lead to defect association or clustering, therefore limiting their mobility [90–92], as has been proven by aliovalent substitution in bulk material [93]. In some cases, the combination of an insulating material, such as Al_2O_3, with Gd-doped ceria electrolyte material in the form of a nanocomposite has been proven to prevent the building up of predominant electronic conductivity by acting as a trap for the generated electrons produced by the reduction of Ce [94].

Multilayers of ionic conducting oxide materials

One of the first evidences of interfacial effects between two different oxides having an important role in enhancing the oxide ionic conductivity was reported by Azad et al. [95] in gadolinia-doped ceria and zirconia multilayers deposited by MBE on Al_2O_3 (0001) substrates. A cross section of the heterostructure is shown in Fig. 8. In such multilayers, the oxygen ion conductivity was increased about one order of magnitude at 350 °C, in comparison to bulk materials.

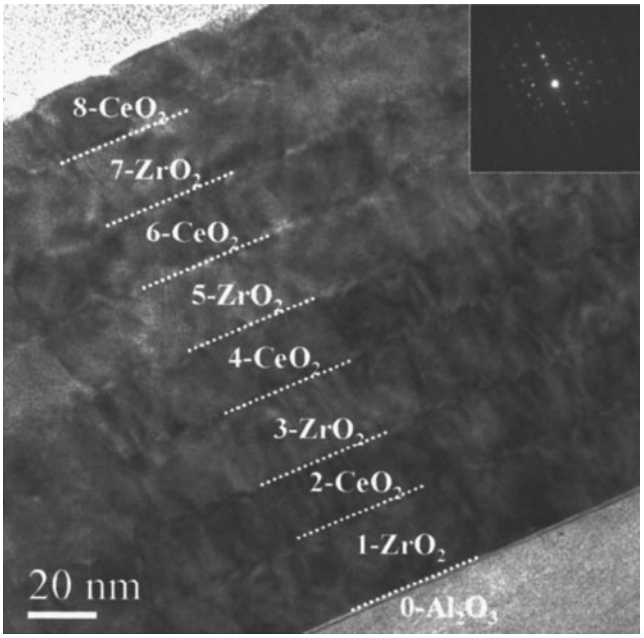

Fig. 8 TEM image of the cross section of an ionic conducting Gd-doped CeO_2/ZrO_2 multilayer deposited on $Al_2O_3(0001)$ single-crystal substrate. Reproduced with permission from [95]. Copyright 2005, American Institute of Physics

Besides, the conductivity enhancement was proportional to the number of interfaces, which evidenced the interface effect. However, the short Debye length in these oxides ruled out the possibility of space charge effects, and the authors therefore suggested the strain or the presence of extended defects as a possible explanation for the conductivity enhancement.

An even greater enhancement of about two orders of magnitude in the electrical conductivity was also observed by Kosacki et al. in highly textured (30 nm) CeO_2/(20 nm) 20% Sm-doped CeO_2 multilayers [96] with a progressive reduction of the activation energy with the number of interfaces from 0.63 eV (for bulk doped material) to 0.46 eV (for a multilayer with 400 periods). However, it was never fully proven that the conductivity enhancement was purely ionic or that the electronic conductivity became predominant due to a reduced enthalpy for oxygen vacancy formation induced by the nanometric CeO_2 layer thickness, in the same way as reported by Suzuki et al. for pure CeO_2 nanocrystalline films [72]. A very recent work reported by Perkins et al. on the same type of CeO_2/(20 nm) 15% Sm-doped CeO_2 epitaxial multilayers deposited on MgO (100) substrates by PLD [97] showed ionic conductivities values very similar to those corresponding to the bulk material. In this case, in order to relax the epitaxial strain and thus eliminate that contribution to the conductivity, the films had been deliberately grown onto a buffer layer. Therefore, this last work points towards the role of strain or of the defects generated in the films associated to the epitaxial strain, rather than to the space charge effects, as the main cause for the ionic or electronic conductivity enhancement in this combination of materials. In a similar way, a recent report by Sanna et al. [98] showed an increase of about one order of magnitude in the conductivity of epitaxial Sm-doped CeO_2/YSZ strained multilayers obtained by PLD on MgO (100) single-crystal substrates, supporting this assumption. The study of the pO_2 dependence in Fig. 9 evidences not only the enhancement of both the ionic conductivity at high pO_2 values, but also of the *n*-type electronic conductivity at low pO_2 values, in direct relation to the number of interfaces in the heterostructure.

Strain effects: effect on mobility

In oxide conducting materials, the increase of carrier concentration has serious limitations. However, the low carrier mobilities could be enhanced by some subtle structural modifications, which would induce variations in the interatomic distances, reducing the energy barrier for oxygen hopping along the diffusion paths. This enhancement has already been demonstrated by modifying the radius of homovalent substitutional cations [99]. In a similar way, it has also been demonstrated that, in thin films submitted to large biaxial stress (of the order of tenths of GPa) generated by the epitaxial growth onto a single-crystal substrate with different cell parameter, the strained structure may induce variations in the ionic mobility. However, depending on the elasticity parameters of the material, a strain larger than a few percent cannot be maintained. The accumulated elastic energy is generally released by the formation of dislocations (or other type of

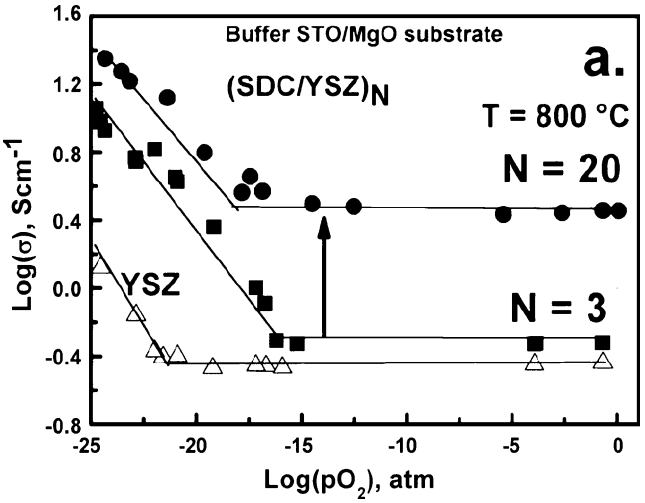

Fig. 9 Conductivity dependence on oxygen partial pressure in epitaxial Sm-doped CeO_2/YSZ heterostructures. Reproduced with permission from [98] © 2010 Wiley-VCH Verlag GmbH & Co. KGaA, Weinheim

defects, as has been discussed in a previous paragraph), and the structure recovers its equilibrium values. In fluorites such as YSZ or CeO_2 combined with different types of insulating oxides (Lu_2O_3, Sc_2O_3, Y_2O_3, Al_2O_3 and MgO) in the form of epitaxial multilayers grown by PLD, it has been demonstrated that the formation of a coherent interface between structures with different cell parameters induces a variation of the ionic mobility. The induced biaxial strain, either tensile (about +3% mismatch in YSZ/Y_2O_3) or compressive (−4% mismatch in YSZ/Sc_2O_3) in a region with a certain extent across the interface, would increase or reduce the interface conductivity, respectively, when compared with better matching structures (about 1% mismatch in YSZ/Lu_2O_3), where the YSZ ionic conductivity approaches that of the bulk material. This has been shown in several studies by J. Janek's group from Giessen Univ. [100–102], and those results are depicted in Fig. 10. A simple model just taking into account the elastic properties of YSZ, relating the volume ratio of the strained material with a volume increase and with a reduction of the activation energy for the oxygen vacancy migration, seems to consistently account for the observed effect.

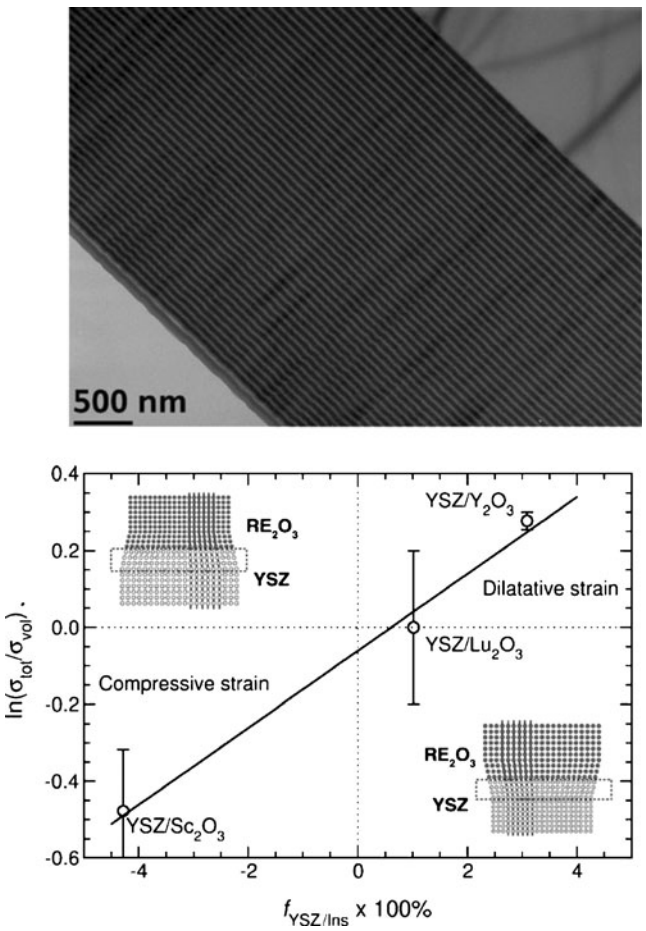

Fig. 10 (*Top*) TEM cross section of a 50×(YSZ/Sc_2O_3) multilayer deposited by PLD on an Al_2O_3(0001) single crystal. (*Bottom*) Film conductivity deviation from bulk behaviour for different heterostructures combining YSZ and RE_2O_3 (RE=Y, Sc and Lu). Reproduced with permission from [102] Royal Society of Chemistry © 2010

However, some authors point to the possibility that the generation of a large density of defects, such as dislocations in semi-coherent heterostructures or boundaries between columnar grains, may produce fast ionic diffusion paths, as attributed in the case of CSZ/Al_2O_3 multilayers reported by Peters et al., where about two orders of magnitude increase in the conductivity were observed [103]. Similarly, a more recent report by Sillassen et al. on YSZ epitaxial single layers deposited by sputtering on MgO (110) substrate [104] (with a very large mismatch of about +18%) showed an increase in the conductivity of about three orders of magnitude. The absence of grain boundaries made the authors associate the ionic conductivity to the presence of a dense array of misfit dislocations generated, accounting for the large mismatch.

Other studies on Gd-doped CeO_2 epitaxial layers deposited by PLD on MgO (100) reported by Chen et al., growing on a cube-on-cube arrangement with an extremely large mismatch of about 28% and therefore expected to have a high density of misfit dislocations, did not show any particular enhancement of the ionic conductivity with respect to the bulk material [105]. These results demonstrate that not only the presence of dislocations but also the characteristics of those defects may be effective in producing fast oxide ionic diffusion paths.

The most astonishing results were reported by Garcia-Barriocanal et al. in STO (100)/YSZ (100) epitaxial multilayers deposited by magnetron sputtering [106] in which an enhancement in the ionic conductivity of about eight orders of magnitude was observed. The authors attributed the enhancement to a particular opened structure of the fluorite induced by the large tensile strain of YSZ at the interface. Although there have been some theoretical studies by first principles supporting this idea [107], these results have raised certain controversy within the solid-state ionics community about whether the conductivity enhancement in YSZ/STO system has a pure ionic character [108, 109] or whether it is related to an electronic conductivity induced by doping the STO substrate with acceptor impurities [108]. Another study on YSZ/STO multilayers deposited by PLD reported by Cavallaro et al. [110] has given a similar conductivity enhancement of several orders of magnitude. However, *p*-type conductivity dependence on pO_2 with exponent of about −1/4, along with the measurement of no enhancement in the oxygen diffusion along the interface direction by means of isotopic oxygen exchange depth profile experiments, has evidenced the electronic nature of the transport mechanism in such system and related it to the possible formation of a highly conducting perovskite-type phase by interdiffusion at the interface.

Thin-film MIEC cathodes

In addition to the general stability and compatibility requirements of any SOFC material, those used as cathode electrodes need to have high electronic conductivity under oxidising conditions and a good catalytic activity toward promoting oxygen dissociation [111]. Current research in the field is mainly being directed toward materials with mixed ionic–electronic transport properties (MIEC), whose use would permit lowering the operation temperature of the cell to the range of 500–700 °C. The state-of-the-art cathode used at higher temperatures, the perovskite LSM, has a limited performance at the intermediate operation temperatures, and therefore substitute materials with improved properties should be identified. By using materials with high ionic conductivity in addition to the electronic contribution, the triple-phase boundary zone is effectively broadened to include the entire surface of the MIEC and, consequently, the polarisation resistance can be lowered.

Materials with the perovskite or related structures dominate the field, mainly including three families of oxides: single perovskites, Ruddlesden–Popper (RP) phases and layered double-perovskite phases. For a detailed description on recent advances on new cathode materials, the reader is referred to the comprehensive reviews by Orera and Slater [111], Jacobson [112], Sun et al. [113] and Tarancón et al. [114]. There have been some recent attempts to fabricate composite cermet cathodes in the form of thin films by combining pure ionic and electronic conducting materials, such as the vertically aligned LSCO/CGO nanocomposite films deposited by PLD by Yoon et al. [115], which have been already successfully tested in symmetric cells. Figure 11 shows the microstructure of such composite electrodes.

Dense thin films have been extensively used to prepare novel electrode compositions and structures for use in fundamental reaction mechanism and electrochemical measurements [116–134] and, as they are optimal materials with a well-defined structure, as model materials for the study of the oxygen surface exchange and bulk diffusion properties of these mixed conductors [119, 135, 136]. Otherwise, in the case of porous bulk samples, the true values of the surface exchange coefficient and diffusivity are actually masked, as they are influenced by non-kinetic material properties (such as density, porosity, etc.). The information extracted from these 'model materials' is key in the design of optimum electrode morphologies. Also, as pointed out by Beckel et al.[1], thin films can also be utilised to increase the performance of SOFC cathodes in miniaturised systems (μSOFC). Examples and details of thin-film cathodes for micro-solid oxide fuel cells can be found in the authors' review article. To date, only a couple of examples of half cells with an epitaxial cathode film on an epitaxial electrolyte substrate have been reported. In such a configuration, the cathode material can be grown to take advantage of its maximum transport direction and, ideally, could be strain-tuned to further boost its MIEC properties.

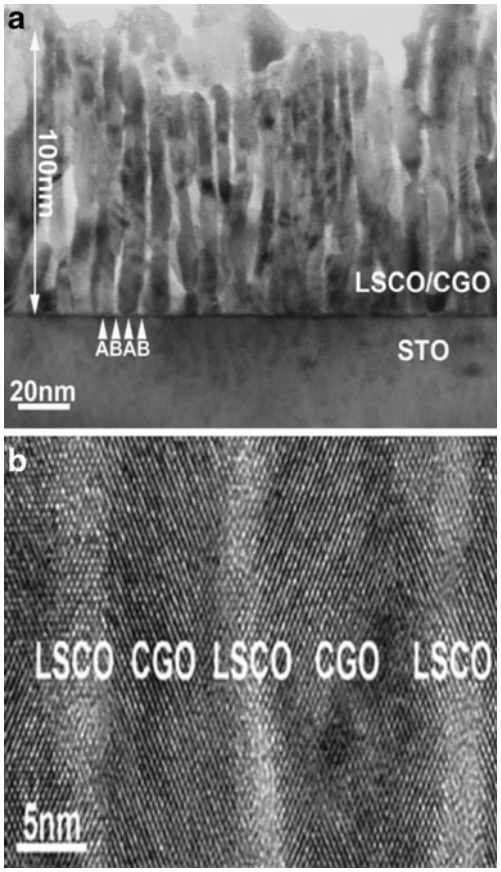

Fig. 11 Cross section of PLD deposited LSCO/CGO vertically ordered nanocomposite cathodes. Low and high magnification (*top* and *bottom*, respectively). Reproduced with permission from [115] © 2009, John Wiley and Sons

Perovskite-type epitaxial films

The number of studies on epitaxial thin films of potential cathode materials is still rather scarce, and these have been mainly been carried out for perovskite-type materials [10, 26, 32, 137–139].

For most of the perovskite materials used such as cathodes in SOFCs, the A site cation of the ABO_3 structure is a mixture of rare and alkaline earths (such as La and Sr, Ca or Ba), while the *B*-site cation is a reducible transition metal such as Mn, Fe, Co or Ni (or a mixture thereof) [113]. Consequently, in most cases, the *B*-site cation usually provides a redox catalytic mechanism. A large and stable number of oxygen ion vacancies can be introduced at the operating conditions of the fuel cell by varying the *A*- and

B-site cations and hence increasing significantly the bulk ionic oxygen transport.

Epitaxial $La_{0.5}Sr_{0.5}CoO_{3-\delta}$ film formation was first reported on the $LaAlO_3$ substrate by Chen et al. [137], who determined its oxygen surface exchange coefficient from electrical conductivity relaxation measurements. The measured values of k_{chem} were very low compared with the values for bulk polycrystal materials, consistent with the observation in literature for LSCO single crystal. Contrary to these results, O' et al. have very recently published a markedly increased oxygen exchange by up to two orders of magnitude relative to the bulk for $La_{0.8}Sr_{0.2}CoO_{3-\delta}$/GDC/YSZ (001) [139]. They attribute this behaviour to increased oxygen vacancy concentrations in the films, in which physical origin is not clearly understood. They suggest that cation defects/vacancies and/or strains are more likely to occur near the epitaxial LSC/GDC interface, which may stabilise more oxygen vacancies and thus enhance the oxygen surface kinetics. This constitutes the first report in which epitaxial oxide films exhibit greatly enhanced surface kinetics and, although a better understanding is highly required, the findings illustrate the potential to promote oxygen activity on selected heterostructured oxide films and provide new strategies to design highly active catalysts for applications in solid oxide fuel cells.

In two previous works, Mori et al. deposited epitaxial $La_{0.8}Sr_{0.2}CoO_{3-\delta}$, $La_{0.8}Sr_{0.2}MnO_3$ (LSM) and $Y_{0.5}Ca_{0.5}MnO_3$ (YCM) thin films with the perovskite structure on YSZ substrates of different orientations and studied their electrochemical properties [10, 31]. The film orientations depended on the plane cut of YSZ substrate. Differences in the resistivity and activation energies were found to depend on the lattice misfit, surface structure and surface morphology, but further studies should be carried out to clarify the relationship between the surface structure and the electrochemical properties. LSM epitaxial films have also been used by Fister et al. to study strontium surface segregation using in situ synchrotron measurements of total reflection X-ray fluorescence [138]. 001-oriented $La_{0.7}Sr_{0.3}MnO_3$ thin films were grown by PLD on $DyScO_3$ (101) and $NdGaO_3$ (101) substrates and measured over a wide range of temperatures and oxygen partial pressures. The strontium surface concentration was observed to increase with decreasing pO_2, suggesting that the surface oxygen vacancy concentration plays a significant role in controlling the degree of segregation. In contrast, the $La_{0.7}Sr_{0.3}MnO_3$ film thickness and epitaxial strain state had little impact on segregation behaviour.

Another perovskite material which presents improved properties when prepared as high-quality epitaxial thin films is $Ba_{0.5}Sr_{0.5}Co_{0.8}Fe_{0.2}O_{3-\delta}$ (BSCF). The electrical conductivity of the thin films prepared by PLD on single-crystal $NdGaO_3$ (110) showed different activation energies and higher general conductivity [26] when compared to polycrystalline bulk values. In this case, the measured surface exchange coefficients are in the same range of magnitude as those measured for polycrystalline BSCF samples.

Ruddlesden–Popper phases

The homologous series of compounds with the general formula $A_{n+1}M_nO_{3n+1}$ that are structurally similar to the titanates, $Sr_{n+1}Ti_nO_{3n+1}$, reported by Ruddlesden and Popper in 1958 [140] are referred to as RP phases. The structure of the RP phases is made up of n consecutive perovskite layers $(AMO_3)_n$, alternating with rock-salt layers (AO), along the crystallographic c-axis direction, so their formula can be represented by $(AO)(AMO_3)_n$, where n represents the number of connected layers of vertex sharing MO_6 octahedra. Of particular interest in the case materials for SOFC cathodes are the $n=1$ members of the family, particularly those based on $La_2NiO_{4+\delta}$, which can accommodate oxygen interstitials in the rock-salt layers, giving as result fast ion conduction and hence potential application at intermediate temperatures. Given their layered structure, the physical properties of the $n=1$, 2 and 3 phases are expected to be highly anisotropic.

Within the RP family and motivated by their superconductivity properties, Shinomori et al. [11] were the first to report on the synthesis of epitaxial thin films of Sr-doped lanthanum nickelate ($La_{2-x}Sr_xNiO_4$) on two different substrates and to measure their anisotropic electronic properties at low temperatures, as has been previously explained in 'Transport anisotropy'. The synthesis of undoped c-axis-oriented $La_2NiO_{4+\delta}$ epitaxial thin films has been reported by two different groups: by Kim et al., who deposited the films on $LaAlO_3$ (001) substrates using PLD [23], and Burriel et al., who deposited the films on $SrTiO_3$ (100) and $NdGaO_3$ (110) substrates by pulsed-injection metal-organic chemical vapour deposition [141, 142]. In this second case, the electrical conductivity along the a–b plane increased by decreasing the film thickness, reaching values of 475 S/cm for 33-nm-thick films [142, 143], higher than the values reported for bulk samples and even for single crystals. An important role of the absolute strain on the transport properties of this material was suggested and related to the structural evolution observed from a strained structure to a more relaxed one upon thickness increase. A complementary work from Burriel et al. [28] confirmed an anisotropic behaviour of the oxygen diffusion and surface exchange of the $La_2NiO_{4+\delta}$ epitaxial thin films, showing two to three orders of magnitude larger values along the a–b plane than along the c-axis (as shown in Fig. 12). For this purpose, the authors developed and

validated a new methodology for measuring the surface exchange and oxygen diffusion properties of thin films in two perpendicular directions by the isotope exchange and depth profiling (IEDP) method, as has been explained in 'Epitaxial strain'. Another finding of this work was the increase of the diffusion coefficients (both along the *c*-axis and along the *a*–*b* plane) with film thickness, i.e. as the strain in the film is released. Contrary, the thickness did not have a direct effect on the surface exchange coefficients.

In an attempt to obtain thin films of the higher members of the Ruddlesden–Popper series ($La_{n+1}Ni_nO_{3n+1}$, $n>1$), Burriel et al. [144] varied and controlled the La/Ni stoichiometry of the films. In addition to epitaxial La_2NiO_4 ($n=1$) and $LaNiO_3$ ($n=\infty$) pure phases, for intermediate values of La/Ni composition, films with a microstructure consisting of a disordered stacking of nanodomains with progressively increasing average n value were obtained. Similar to the bulk samples, the electronic conductivity of the nanostructured films increased with the measured average n value, opening the possibility of preparing new mixed ionic and electronic conducting nanocomposite thin films with tailored properties, although no information about ionic conductivity in those phases has been reported to date.

Despite a high epitaxial mismatch of 9.98%, Yamada et al. [30] were able to deposit very thin (110)-oriented epitaxial layers (*approximately* 14 nm) of $Nd_2NiO_{4+\delta}$ on a (100) YSZ single crystal by PLD, obtaining the first reported heteroepitaxial SOFC system. The authors claim that this K_2NiF_4-type structure might have some inherent flexibility that allows epitaxial growth despite its large mismatch. By impedance spectroscopy, the authors measured a large activation energy for oxygen diffusion along the *a*–*b* plane, which they think could be related to the shrinkage of the bottleneck for the interstitial oxide ion diffusion, resulting from the significantly small measured *c* (in-plane) and from an expanded *a* (out-of-plane) cell parameter for the Nd_2NiO_4 film. This is an example of how the cathode properties can be optimised by preparing highly textured or epitaxial thin films with the planes or channels of maximum ionic transport aligned with the oxygen diffusion direction. This is especially convenient in the case of micro-fuel cells in which the cathode is a thin-film layer.

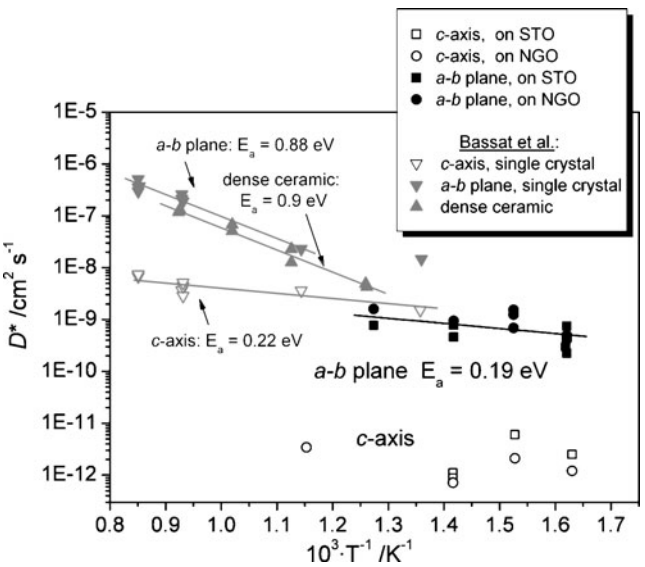

Fig. 12 Arrhenius plot of the *c*-axis diffusivity in the zone close to the film surface (D_{c1}^*) and of the *ab* plane diffusivity (D_{ab}^*) for La_2NiO_4 films deposited on STO and on NGO and comparison with the literature data for La_2NiO_4 single crystal and dense ceramics. Reproduced with permission from [28] Royal Society of Chemistry © 2008

Double perovskites and layered ferrites

Ordered double perovskites with general formula $AA'B_2O_{5+x}$, where A is a rare earth, A' an alkaline earth and B either Co or Mn ($GdBaCo_2O_{5+\delta}$ structure shown as example in Fig. 2), have been recently proposed as the next-generation cathode materials for intermediate- to low-temperature operation due to their high electronic conductivity and enhanced oxygen surface exchange rate and transport properties [114]. These layered cobaltites are being actively studied, not only due to their mixed conducting properties but also due to their magnetic properties, having shown phenomena such as a metal–insulator transition or colossal magnetoresistance effect [145]. The properties of these compounds depend strongly on the oxygen content and oxygen vacancy ordering, as well as on the ordering of the A and A' cations. The structure ordering shown in Fig. 2, in which rare earth and alkali-earth ions occupy alternate (001) layers and oxygen vacancies are mainly located in the rare earth planes forming channels along the *a*-axis, occurs for each compound for a certain range of oxygen stoichiometry and is thought to be responsible for the high oxygen diffusivity values.

As these materials can be prepared with A site cation-ordered or cation-disordered structure at the same composition, their growth as epitaxial films has proven to be complicated. In addition, due to the defined oxygen content window at which the ordered oxygen vacancies appear, along with the peculiarities of vapour-phase growth, the selection of the appropriate substrate and deposition conditions has to be done very carefully in order to obtain epitaxial films of one sole domain orientation. A very nice example of how the preparation conditions can affect the film microstructure and properties of the films can be found in the work done by Kasper et al.[146] for epitaxial $TbBaCo_2O_{5+x}$ films. The authors managed to grow *c*-axis-oriented epitaxial films on $SrTiO_3$ (STO) and (La, Sr)(Al, Ta)O_3 (LSAT) substrates, while a mixture of *c*- and *a*(*b*)-oriented crystallites or *c*-oriented films with a large 'out-of-

plane' mosaic was always obtained on $LaSrAlO_4$ and $LaSrGaO_4$ substrates, independent of substrate temperature and oxygen pressure during deposition. They also found that the phase with perovskite structure only developed if the oxygen pressure in the chamber during deposition was larger than 5×10^{-3} mbar and that the superstructural reflections showing the ordering of the cations only appeared in films grown at substrate temperatures larger than 897 °C. Additionally, oxygen vacancy ordering was found for identical deposition conditions only if the cooling rate after deposition was very low (1 K/min).

The first successful attempt on the growth of double perovskites epitaxial films was carried out by Kim et al. [147] and Yuan et al. [148], who synthesised $PrBaCo_2O_{5+x}$(PBCO) thin films by PLD on (001) $SrTiO_3$, finding the coexistence of two domain structures in the films [147, 148]. The authors measured the oxygen exchange kinetics of thin films by electrical conductivity relaxation (ECR) and by oxygen IEDP, revealing high electronic conductivity and rapid surface exchange kinetics. The same group of authors have very recently reported on the epitaxial growth of $LaBaCo_2O_{5+x}$ thin films on (001) $LaAlO_3$ single-crystal substrates by PLD [149, 150]. The films were claimed to be *c*-axis-oriented with very weak superstructure ordering reflections appearing along this axis, which could be either due to cation or oxygen vacancy ordering. After a treatment in hydrogen, the epitaxial nature was maintained while the superlattice peaks disappeared. The chemical dynamic studies on the films revealed a drastic change in resistance with a change of redox environment, within short response times, suggesting an extraordinary sensitivity to reducing oxidising environment and an exceedingly fast surface exchange rate. The results indicate that, at low oxygen partial pressure, the extension of oxygen deficiency is an essential factor to the high-temperature physical properties of $LaBaCo_2O_{5+x}$ and suggest its potential application as a cathode material in intermediate-temperature SOFCs or as a chemical sensor device for reducing environments at high temperature.

The possibility of controlling the growth on a unit cell level for another double cobaltite compound, namely $NdBaCo_2O_{5+\delta}$, has been achieved by Grygiel et al. [151] for epitaxial films on (001) $SrTiO_3$ substrates (Fig. 13 shows a high-resolution transmission electron microscopy (TEM) image of an ordered $NdBaCo_2O_{5+\delta}$ film exhibiting doubling of the out-of-plane lattice parameter). By adjusting the growth kinetics via control of temperature and laser energy, cation-ordered units (with double cell parameter) or cation-disordered units (with single unit cell parameter) were selectively incorporated into the $NdBaCo_2O_{5+\delta}$ structure while retaining layer-by-layer growth. This work opens routes for systematically depositing heterostructures of these complex oxides with cation order. The electrochemical properties of these epitaxial double perovskite layers are still to be evaluated.

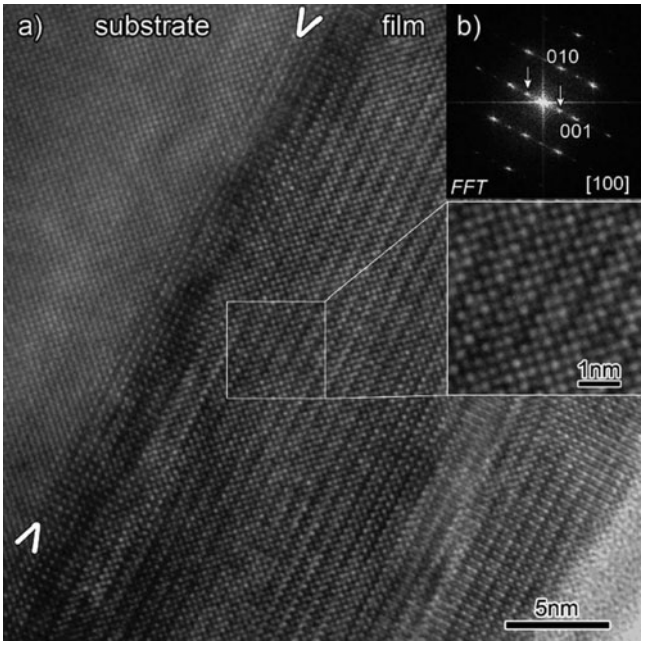

Fig. 13 **a** High-resolution TEM image for a cross section of a 34-nm ordered $NdBaCo_2O_{5+\delta}$ film grown by conventional mode. The film/substrate interface is highlighted by two *arrows*. **b** Fourier transform where *arrows* show the doubling of the lattice parameter along the [001] direction. Reproduced with permission from [151] American Chemical Society © 2010

Finally, the first $GdBaCo_2O_{5+\delta}$ (GBCO) growth studies by PLD [152] have shown the microstructural complexity of this compound in an epitaxial thin-film form. The epitaxial GBCO films prepared mainly consisted of single- and double-perovskite regions presenting changes in the film orientation from *a(b)*- to *c*-oriented upon deposition temperature increase. In addition, the presence of a high density of planar defects, consisting of additional rock-salt GdO layers (as in Ruddlesden Popper phases), was generated by a deviation in the composition of the films. The film electronic conductivities seem to be mainly correlated with the cation composition; so, the larger the deviation from stoichiometric composition, the lower is the conductivity. Despite the presence of defects, the conductivity of the films, with values as high as 800 S/cm at 330 °C in 1 atm O_2, is considered very promising for their application as cathodes in intermediate-temperature SOFCs. Although it is clear that further investigations are required, the possibility of tailoring the electronic conductivity by inducing microstructural defects could open a new field of research in thin films.

Another anisotropic material with layered structure which had been proposed as MIEC for IT-SOFC cathode is $Sr_4Fe_6O_{13}$, whose structure can be considered as a stacking of $SrFeO_3$ perovskite blocks with FeO_6 in

octahedral coordination separated by a double layer of FeO_4–FeO_5 polyhedra. A comprehensive study carried out by Solis et al. [18, 153] showed a strong variation of the transport properties by varying the film thickness of *b*-axis-oriented epitaxial thin films grown on three different substrates ($SrTiO_3$, $NdGaO_3$ and $LaAlO_3$), showing an unexpected enhancement for strained films. The strain accommodation was found to vary as a function of film thickness and of the substrate material, causing different types of defects in the film microstructure, as well as variations in the oxygen anion content and ordering. Unfortunately, so far, there has been no experimental evidence of enhanced ionic conductivity predicted by theoretical studies [154] for this structure.

Thin-film anodes

In the SOFC anode, the fuel oxidises electrochemically with the oxide ions supplied through the electrolyte membrane. The conditions that the anode material has to fulfil, some of them matching those of the cathode, are mainly that (1) the material should be electronic conducting under the typical reducing conditions for the fuel atmosphere to collect the electrons produced in the fuel oxidation and conduct them to the external circuit; (2) ideally, the material would also be ionic conducting in order to extend the interface between the electrolyte, the electronic conductor and the fuel gas phase (triple-phase boundary); (3) it has to be catalytically active for that oxidation and ideally for hydrocarbon cracking; (4) it should be chemically stable at the extreme conditions of the cathode (to prevent performance loss due to catalyst poisoning by sulphur or graphitic carbon formation).

Current-state SOFCs do not use thin-film anodes. There are very few works dealing with thin-film anodes, and most of them are model studies for the catalytic oxidation of hydrocarbons and the combination of metal oxides (such as doped CeO_2) with small charges of metal catalysts (see for instance [155–157]). In most of the cases (particularly when using H_2 as fuel), it is generally accepted that the thickness influence in the charge transport processes at the anode does not limit the electrochemical performance of the total cell. Therefore, the typical choice for present SOFCs are based in anode-supported cells with the anode being thick enough to mechanically maintain the integrity of the cell. Conventional Ni–YSZ anodes have been prepared by sintering at high temperatures over 1,300 °C. Obviously, this process is not compatible with the preparation of the anode layer on the thin-film electrolyte.

However, recent interest in developing either metal-supported (porous ferritic steel or Ni alloys) [158] or self-supported SOFC platforms, with extremely low thermal mass [1, 159–163], requires the use of thin layers for all components. In this sense, there have been some efforts to develop thin-film nanocomposite anodes [156, 164–169]. Particularly interesting is the fabrication of Ni:Gd-substituted CeO_2 thin-film cermet reported by Infortuna et al. [170], obtained by pulsed laser deposition from the direct ablation of mixed NiO–Gd:CeO_2 targets. The cermet showed a stable microstructure with an intimate dispersion of interconnected Ni particles in a porous electrolyte matrix, avoiding Ni coarsening up to an operation temperature of 500 °C. Other attempts to grow thin films suitable as anode material are mainly related to Pt [171] or Ni deposition [172]. In some cases and particularly when using metallic supports, it is necessary to use thin diffusion barriers to avoid Cr or Fe diffusion into the Ni-containing anode layer [173] or additional thin activation layers, with a finer porous structure which guarantee the catalytic activity for the hydrocarbon oxidation [174]. Concerning the anode element, there is still substantial place for the development of new Ni-free compositions and structures that provide high power density at low temperature with low degradation rate and tolerance to sulphur poisoning and coke formation. In this sense, perovskite-related single-phase materials such as Y-substituted $SrTiO_3$ [175–179], $La_{0.75}Sr_{0.25}Cr_{0.5}Mn_{0.5}O_3$ [180], tungstate bronzes or pyrochlores [181] have demonstrated considerable electronic conductivity and redox capabilities while maintaining sulphur tolerance and are excellent candidates to be explored in thin-film form.

Conclusions and future perspectives

At the moment, research on epitaxial thin-film materials for electrolyte and electrode applications truly constitutes a ‘hot topic’ within the solid-state materials community, clearly reflected by the increasing number of articles related to the area which have been published in the last years. Most of the studies included in the present review concern the use of epitaxial films for fundamental research on the intrinsic properties of materials for IT-SOFCs. In addition, it has been shown that important materials properties, such as the oxide ionic and electronic transport, along with the oxygen surface exchange, can be tailored by selecting the substrate and the deposition conditions used for preparing epitaxial films and heterostructures.

Concerning SOFC devices, the present application of thin films is limited to polycrystalline or highly textured thin deposits. However, there are considerable expectations of incorporating epitaxial films and heterostructures in future monolithic SOFC devices and particularly in μSOFC platforms. In μSOFCs, the reduction of the thickness of the overall cell components allows, on the one hand, minimisation of the ohmic losses due to the limited charge transport through the elements, particularly at lower

operating temperatures (from 400 to 600 °C) and, on the other hand, reduction of the thermal mass of the active cell volume, reducing as a result the thermal energy losses and gaining portability. Several comprehensive reviews dealing with μSOFCs' fundamental and more technological aspects can be found in [1, 159–162, 182–184].

In summary, although the number of research studies concerning epitaxial thin films for SOFC materials is still rather limited, especially in the case of actual SOFC devices, it can be already foreseen that the versatility of the epitaxial growth for both fundamental studies and final applications is enormous, and it is expected to be an area of intense research efforts during the next years.

Acknowledgements The authors would like to acknowledge the Spanish Ministry of Education for funding through different projects (MAT2008-03501, Consolider-Ingenio CSD2008-024). MB would like to acknowledge King Abdullah University of Science and Technology (KAUST) for the funding provided through a research grant.

References

1. Beckel D et al (2007) Thin films for micro solid oxide fuel cells. J Power Sources 173(1):325–345
2. Kreuer KD (2003) Proton conducting oxides. Annu Rev Mater Res 33:333–359
3. Freund LB, Suresh S (2003) Thin film materials: stress, defect formation, and surface evolution. Cambridge University Press, Cambridge
4. Hegde MS (2001) Epitaxial oxide thin films by pulsed laser deposition: retrospect and prospect. J Chem Sci 113(5):445–458
5. Ohring M (2002) Characterization of thin films and surfaces, in materials science of thin films, 2nd edn. Academic, San Diego, pp 559–640
6. Habermeier H-U (2007) Thin films of perovskite-type complex oxides. Mater Today 10(10):34–43
7. Kumigashira H et al (2004) Surface electronic structures of terminating-layer-controlled $La_{0.6}Sr_{0.4}MnO_3$ thin films studied by in situ synchrotron-radiation photoemission spectroscopy. J Magn Magn Mater 272–276(Part 2):1120–1121
8. Kawasaki M et al (1994) Atomic control of the $SrTiO_3$ crystal surface. Science 266(5190):1540–1542
9. Koster G et al (1998) Quasi-ideal strontium titanate crystal surfaces through formation of strontium hydroxide. Appl Phys Lett 73(20):2920–2922
10. Mori D et al (2006) Synthesis, structure, and electrochemical properties of epitaxial perovskite $La_{0.8}Sr_{0.2}CoO_3$ film on YSZ substrate. Solid State Ionics 177(5–6):535–540
11. Shinomori S, Kawasaki M, Tokura Y (2002) Orientation-controlled epitaxy and anisotropic properties of $La_{2-x}Sr_xNiO_4$ with $0.5 <= x <= 1.5$ covering the insulator-metal transition. Appl Phys Lett 80(4):574–576
12. Inoue S et al (2010) Anisotropic oxygen diffusion at low temperature in perovskite-structure iron oxides. Nat Chem 2 (3):213–217
13. Guo X, Maier J (2009) Ionically conducting two-dimensional heterostructures. Adv Mater 21(25–26):2619–2631
14. Riess I (1996) Review of the limitation of the Hebb–Wagner polarization method for measuring partial conductivities in mixed ionic electronic conductors. Solid State Ionics 91(3–4): 221–232
15. Gellings PJ, Bouwmeester HJM (1997) The CRC handbook of solid state electrochemistry. CRC, Boca Raton, p 630
16. Chiang YM et al (1996) Defect and transport properties of nanocrystalline CeO_{2-x}. Appl Phys Lett 69(2):185–187
17. Rothschild A et al (2006) Electronic structure, defect chemistry, and transport properties of $SrTi_{1-x}Fe_xO_{3-y}$ solid solutions. Chem Mater 18(16):3651–3659
18. Solis C et al (2010) Defect structure, charge transport mechanisms, and strain effects in $Sr_4Fe_6O_{12+\delta}$ epitaxial thin films. Chem Mater 22(4):1452–1461
19. Patrakeev MV et al (2003) Electron/hole and ion transport in $La_{1-x}Sr_xFeO_{3-\delta}$. J Solid State Chem 172(1):219–231
20. Stevenson JW et al (1996) Electrochemical properties of mixed conducting perovskites $La(1-x)M(x)Co(1-y)Fe(y)O(3-\delta)$ (M= Sr, Ba, Ca). J Electrochem Soc 143(9):2722–2729
21. Tai LW et al (1995) Structure and electrical properties of $La_{1-x}Sr_xCo_{1-y}Fe_yO_{3.1}$. The system $La_{0.8}Sr_{0.2}Co_{1-y}Fe_yO_3$. Solid State Ionics 76(3–4):259–271
22. Maier J (1998) On the correlation of macroscopic and microscopic rate constants in solid state chemistry. Solid State Ionics 112(3–4):197–228
23. Kim G et al (2006) Measurement of oxygen transport kinetics in epitaxial $LaNiO_{4+\delta}$ thin films by electrical conductivity relaxation. Solid State Ionics 177(17–18):1461–1467
24. Tsuchiya M et al (2009) Microstructural effects on electrical conductivity relaxation in nanoscale ceria thin films. J Chem Phys 130(17):174711
25. Tragut C, Härdtl KH (1991) Kinetic behaviour of resistive oxygen sensors. Sensor Actuat B Chem 4(3–4):425–429
26. Burriel M et al (2010) BSCF epitaxial thin films: electrical transport and oxygen surface exchange. Solid State Ionics 181 (13–14):602–608
27. Maier J (2004) Physical chemistry of ionic materials. Ions and electrons in solids. Wiley, England, p 538
28. Burriel M et al (2008) Anisotropic oxygen diffusion properties in epitaxial thin films of $La_2NiO_{4+\delta}$. J Mater Chem 18(4):416–422
29. Crank J (1975) The mathematics of diffusion. Oxford University Press, Oxford
30. Yamada A et al (2008) Ruddlesden–Popper-type epitaxial film as oxygen electrode for solid-oxide fuel cells. Adv Mater 20 (21):4124–4128
31. Mori D et al (2007) Synthesis, structure and electrochemical properties of epitaxial perovskite films deposited on YSZ substrate. In: Eguchi K et al (eds) Solid oxide fuel cells, vol 10. Electrochemical Society, Pennington, pp 749–756
32. Badwal SPS, Foger K (1996) Solid oxide electrolyte fuel cell review. Ceram Int 22(3):257–265
33. Brandon NP, Skinner S, Steele BCH (2003) Recent advances in materials for fuel cells. Annu Rev Mater Res 33:183–213
34. Fergus JW (2006) Electrolytes for solid oxide fuel cells. J Power Sources 162(1):30–40
35. Goodenough JB (2003) Oxide-ion electrolytes. Annu Rev Mater Res 33:91–128
36. Haile SM (2003) Fuel cell materials and components. Acta Mater 51(19):5981–6000
37. Ivers-Tiffee E, Weber A, Herbstritt D (2001) Materials and technologies for SOFC-components. J Eur Ceram Soc 21(10–11): 1805–1811
38. Kharton VV et al (2001) Ceria-based materials for solid oxide fuel cells. J Mater Sci 36(5):1105–1117
39. Maricle DL, Swarr TE, Karavolis S (1992) Enhanced ceria—a low-temperature SOFC electrolyte. Solid State Ionics 52(1–3): 173–182

40. Minh NQ (1993) Ceramic fuel-cells. J Am Ceram Soc 76 (3):563–588
41. Mizutani Y et al (1994) Development of high-performance electrolyte in SOFC. Solid State Ionics 72:271–275
42. Ralph JM, Schoeler AC, Krumpelt M (2001) Materials for lower temperature solid oxide fuel cells. J Mater Sci 36 (5):1161–1172
43. Singh P, Minh NQ (2004) Solid oxide fuel cells: technology status. Int J Appl Ceram Tec 1(1):5–15
44. Singhal SC (2000) Advances in solid oxide fuel cell technology. Solid State Ionics 135(1–4):305–313
45. Steele BCH (2000) Materials for IT-SOFC stacks 35 years R&D: the inevitability of gradualness? Solid State Ionics 134(1–2):3–20
46. Baumann FS et al (2006) Impedance spectroscopic study on well-defined (La, Sr)(Co, Fe)$O_{3-\delta}$ model electrodes. Solid State Ionics 177(11–12):1071–1081
47. Fleig J, Maier J (2004) The polarization of mixed conducting SOFC cathodes: effects of surface reaction coefficient, ionic conductivity and geometry. J Eur Ceram Soc 24(6):1343–1347
48. Holtappels P, Bagger C (2002) Fabrication and performance of advanced multi-layer SOFC cathodes. J Eur Ceram Soc 22 (1):41–48
49. Huang KQ et al (1997) Electrode performance test on single ceramic fuel cells using as electrolyte Sr- and Mg-doped $LaGaO_3$. J Electrochem Soc 144(10):3620–3624
50. Jiang SP, Love JG, Apateanu L (2003) Effect of contact between electrode and current collector on the performance of solid oxide fuel cells. Solid State Ionics 160(1–2):15–26
51. Jorgensen MJ, Mogensen M (2001) Impedance of solid oxide fuel cell LSM/YSZ composite cathodes. J Electrochem Soc 148 (5):A433–A442
52. Jorgensen MJ et al (2001) Effect of sintering temperature on microstructure and performance of LSM–YSZ composite cathodes. Solid State Ionics 139(1–2):1–11
53. Kuznecov M et al (2003) Diffusion controlled oxygen transport and stability at the perovskite/electrolyte interface. Solid State Ionics 157(1–4):371–378
54. Lee HY, Oh SM (1996) Origin of cathodic degradation and new phase formation at the $La_{0.9}Sr_{0.1}MnO_3$/YSZ interface. Solid State Ionics 90(1–4):133–140
55. Mauvy F et al (2003) Oxygen electrode reaction on $Nd_2NiO_{4+\delta}$ cathode materials: impedance spectroscopy study. Solid State Ionics 158(1–2):17–28
56. Mitterdorfer A, Gauckler LJ (1998) $La_2Zr_2O_7$ formation and oxygen reduction kinetics of the $La_{0.85}Sr_{0.15}Mn_yO_3$, O^{-2}/YSZ system. Solid State Ionics 111(3–4):185–218
57. Wang SR et al (2002) Performance of a $La_{0.6}Sr_{0.4}Co_{0.8}Fe_{0.2}O_3$-$Ce_{0.8}Gd_{0.2}O_{1.9}$-Ag cathode for ceria electrolyte SOFCs. Solid State Ionics 146(3–4):203–210
58. Zhang XG et al (1999) Ni-SDC cermet anode for medium-temperature solid oxide fuel cell with lanthanum gallate electrolyte. J Power Sources 83(1–2):170–177
59. Zhang XG et al (2000) Interface reactions in the NiO–SDC–LSGM system. Solid State Ionics 133(3–4):153–160
60. Kawada T et al (1992) Reaction between solid oxide fuel-cell materials. Solid State Ionics 50(3–4):189–196
61. Vanroosmalen JAM, Cordfunke EHP (1992) Chemical-reactivity and interdiffusion of (La, Sr)MnO_3 and (Zr, Y)O_2, solid oxide fuel-cell cathode and electrolyte materials. Solid State Ionics 52 (4):303–312
62. Tomida K, Namikawa T, Yamazaki Y (1994) Tensile test of corrugated 8-YSZ thin-films for SOFC. Denki Kagaku 62 (11):1043–1047
63. Steele BCH, Heinzel A (2001) Materials for fuel-cell technologies. Nature 414(6861):345–352
64. Jung W, Hertz JL, Tuller HL (2009) Enhanced ionic conductivity and phase meta-stability of nano-sized thin film yttria-doped zirconia (YDZ). Acta Mater 57(5):1399–1404
65. Kosacki I et al (2004) Surface/interface-related conductivity in nanometer thick YSZ films. Electrochem Solid St 7(12):A459–A461
66. Kosacki I et al (2005) Nanoscale effects on the ionic conductivity in highly textured YSZ thin films. Solid State Ionics 176(13–14): 1319–1326
67. Karthikeyan A, Chang C-L, Ramanathan S (2006) High temperature conductivity studies on nanoscale yttria-doped zirconia thin films and size effects. Appl Phys Lett 89 (18):183116
68. Tschöpe A, Birringer R (2001) Grain size dependence of electrical conductivity in polycrystalline cerium oxide. J Electroceram 7(3):169–177
69. Kim S, Maier J (2002) On the conductivity mechanism of nanocrystalline ceria. J Electrochem Soc 149(10):J73–J83
70. Tschöpe A (2001) Grain size-dependent electrical conductivity of polycrystalline cerium oxide II: space charge model. Solid State Ionics 139(3–4):267–280
71. Lavik EB et al (1997) Nonstoichiometry and electrical conductivity of nanocrystalline CeO. J Electroceram 1(1):7–14
72. Suzuki T, Kosacki I, Anderson HU (2002) Microstructure electrical conductivity relationships in nanocrystalline ceria thin films. Solid State Ionics 151(1–4):111–121
73. Rupp JLM, Gauckler LJ (2006) Microstructures and electrical conductivity of nanocrystalline ceria-based thin films. Solid State Ionics 177(26–32):2513–2518
74. Guo X, Maier J (2001) Grain boundary blocking effect in zirconia: a Schottky barrier analysis. J Electrochem Soc 148(3): E121–E126
75. Rodewald S, Fleig J, Maier J (2001) Microcontact impedance spectroscopy at single grain boundaries in Fe-doped $SrTiO_3$ polycrystals. J Am Ceram Soc 84(3):521–530
76. Fleig J (2002) The grain boundary impedance of random microstructures: numerical simulations and implications for the analysis of experimental data. Solid State Ionics 150(1–2):181–193
77. Abrantes JCC, Labrincha JA, Frade JR (2000) Applicability of the brick layer model to describe the grain boundary properties of strontium titanate ceramics. J Eur Ceram Soc 20(10):1603–1609
78. Fleig J, Maier J (1999) The impedance of ceramics with highly resistive grain boundaries: validity and limits of the brick layer model. J Eur Ceram Soc 19(6–7):693–696
79. Hwang JH, McLachlan DS, Mason TO (1999) Brick layer model analysis of nanoscale-to-microscale cerium dioxide. J Electroceram 3(1):7–16
80. Kidner NJ et al (2008) The brick layer model revisited: introducing the nano-grain composite model. J Am Ceram Soc 91(6):1733–1746
81. Nan CW et al (2001) Grain-boundary-controlled impedances of electroceramics: generalized effective-medium approach and brick-layer model. J Appl Phys 89(7):3955–3959
82. Rupp JLM et al (2009) Crystallization and grain growth kinetics for precipitation-based ceramics: a case study on amorphous ceria thin films from spray pyrolysis. Adv Funct Mater 19 (17):2790–2799
83. Rupp JLM, Infortuna A, Gauckler LJ (2007) Thermodynamic stability of gadolinia-doped ceria thin film electrolytes for micro-solid oxide fuel cells. J Am Ceram Soc 90(6):1792–1797
84. Steele BCH (2000) Appraisal of $Ce_{1-y}Gd_yO_{2-y/2}$ electrolytes for IT-SOFC operation at 500 °C. Solid State Ionics 129(1–4):95–110
85. Wagner C (1972) The electrical conductivity of semi-conductors involving inclusions of another phase. J Phys Chem Solids 33 (5):1051–1059

86. Maier J (1995) Ionic conduction in space charge regions. Prog Solid State Ch 23(3):171–263
87. Sata N et al (2000) Mesoscopic fast ion conduction in nanometre-scale planar heterostructures. Nature 408(6815):9 46–949
88. Sata N et al (2002) Enhanced ionic conductivity and mesoscopic size effects in heterostructures of BaF_2 and CaF_2. Solid State Ionics 154–155:497–502
89. Sata N et al (2007) Synthesis of $La_{0.6}Sr_{0.4}FeO_3/La_{0.6}Sr_{0.4}CoO_3$ mixed ion conducting superlattices by PLD. Solid State Ionics 178(29–30):1563–1567
90. Moore DS, Wright JC (1979) Evidence for cluster control of the defect equilibria in fluorite structure crystals. Chem Phys Lett 66 (1):173–176
91. Gibson IR, Irvine JTS (1996) Study of the order–disorder transition in yttria-stabilised zirconia by neutron diffraction. J Mater Chem 6(5):895–898
92. Goff JP et al (1999) Defect structure of yttria-stabilized zirconia and its influence on the ionic conductivity at elevated temperatures. Phys Rev B 59(22):14202
93. Hohnke DK (1981) Ionic conduction in doped oxides with the fluorite structure. Solid State Ionics 5:531–534
94. Chockalingam R, Amarakoon VRW, Giesche H (2008) Alumina/cerium oxide nano-composite electrolyte for solid oxide fuel cell applications. J Eur Ceram Soc 28(5):959–963
95. Azad S et al (2005) Nanoscale effects on ion conductance of layer-by-layer structures of gadolinia-doped ceria and zirconia. Appl Phys Lett 86(13):131906–131909
96. Kosacki I (2006) Superlattice electrolyte for energy application. Invention disclosure #5-153.1685, February
97. Perkins JM et al (2010) Anomalous oxidation states in multilayers for fuel cell applications. Adv Funct Mater 20(16):2664–2674
98. Sanna S et al (2010) Enhancement of ionic conductivity in Sm-doped ceria/yttria-stabilized zirconia heteroepitaxial structures. Small 6(17):1863–1867
99. Xia X-L, Ouyang J-H, Liu Z-G (2010) Electrical properties of gadolinium–europium zirconate ceramics. J Am Ceram Soc 93 (4):1074–1080
100. Korte C et al (2008) Ionic conductivity and activation energy for oxygen ion transport in superlattices—the semicoherent multilayer system YSZ (ZrO_2+9.5 mol% Y_2O_3)/Y_2O_3. Phys Chem Chem Phys 10(31):4623–4635
101. Korte C et al (2009) Influence of interface structure on mass transport in phase boundaries between different ionic materials. Monatsh Chem 140(9):1069–1080
102. Schichtel N et al (2009) Elastic strain at interfaces and its influence on ionic conductivity in nanoscaled solid electrolyte thin films—theoretical considerations and experimental studies. Phys Chem Chem Phys 11(17):3043–3048
103. Peters A et al (2007) Ionic conductivity and activation energy for oxygen ion transport in superlattices—the multilayer system CSZ (ZrO_2+CaO)/Al_2O_3. Solid State Ionics 178(1–2):67–76
104. Sillassen M et al (2010) Low-temperature superionic conductivity in strained yttria-stabilized zirconia. Adv Funct Mater 20 (13):2071–2076
105. Chen L et al (2003) Electrical properties of a highly oriented, textured thin film of the ionic conductor Gd:$CeO_{2-\delta}$ on (001) MgO. Appl Phys Lett 83(23):4737–4739
106. Garcia-Barriocanal J et al (2008) Colossal ionic conductivity at interfaces of epitaxial ZrO_2:Y_2O_3/$SrTiO_3$ heterostructures. Science 321(5889):676–680
107. Kushima A, Yildiz B (2009) Role of lattice strain and defect chemistry on the oxygen vacancy migration at the (8.3% Y_2O_3–ZrO_2)/$SrTiO_3$ hetero-interface: a first principles study. ECS Trans 25(2):1599–1609
108. Guo X (2009) Comment on "colossal ionic conductivity at interfaces of epitaxial ZrO_2:Y_2O_3/$SrTiO_3$ heterostructures". Science 324(5926):465
109. Garcia-Barriocanal J et al (2009) Response to comment on "Colossal ionic conductivity at interfaces of epitaxial ZrO_2:Y_2O_3/$SrTiO_3$ heterostructures". Science 324(5926):465
110. Cavallaro A et al (2010) Electronic nature of the enhanced conductivity in YSZ–STO multilayers deposited by PLD. Solid State Ionics 181(13–14):592–601
111. Orera A, Slater PR (2009) New chemical systems for solid oxide fuel cells. Chem Mater 22(3):675–690
112. Jacobson AJ (2009) Materials for solid oxide fuel cells. Chem Mater 22(3):660–674
113. Sun C (2010) Cathode materials for solid oxide fuel cells: a review. J Solid State Electr 14(7):1125–1144
114. Tarancon A et al (2010) Advances in layered oxide cathodes for intermediate temperature solid oxide fuel cells. J Mater Chem 20:3799–3813
115. Yoon J et al (2009) Vertically aligned nanocomposite thin films as a cathode/electrolyte interface layer for thin-film solid-oxide fuel cells. Adv Funct Mater 19(24):3868–3873
116. Chen X et al (1999) Structure and conducting properties of $La_{0.5}Sr_{0.5}CoO_{3-\delta}$ films on YSZ. Thin Solid Films 350(1–2):130–137
117. Chen X et al (1999) Pulsed laser deposition of conducting porous La–Sr–Co–O films. Thin Solid Films 342(1–2):61–66
118. Endo A et al (2000) Cathodic reaction mechanism of dense $La_{0.6}Sr_{0.4}CoO_3$ and $La_{0.81}Sr_{0.09}MnO_3$ electrodes for solid oxide fuel cells. Solid State Ionics 135(1–4):353–358
119. Imanishi N et al (2004) Impedance spectroscopy of perovskite air electrodes for SOFC prepared by laser ablation method. Solid State Ionics 174(1–4):245–252
120. Coocia LG et al (1996) Pulsed laser deposition of novel materials for thin film solid oxide fuel cell applications: $Ce_{0.9}Gd_{0.1}O_{1.95}$, $La_{0.7}Sr_{0.3}CoO_y$ and $La_{0.7}Sr_{0.3}Co_{0.2}Fe_{0.8}O_y$. Appl Surf Sci 96–98:795–801
121. Endo A et al (1996) Cathodic reaction mechanism for dense Sr-doped lanthanum manganite electrodes. Solid State Ionics 86–88 (Part 2):1191–1195
122. Endo A et al (1998) Low overvoltage mechanism of high ionic conducting cathode for solid oxide fuel cell. J Electrochem Soc 145(3):L35–L37
123. Mizusaki J, Saito T, Tagawa H (1996) A chemical diffusion-controlled electrode reaction at the compact $La_{1-x}Sr_xMnO_3$/stabilized zirconia interface in oxygen atmospheres. J Electrochem Soc 143(10):3065–3073
124. Ioroi T et al (1997) Preparation of perovskite-type $La_{1-x}Sr_xMnO_3$ films by vapor-phase processes and their electrochemical properties. J Electrochem Soc 144(4):1362–1370
125. Yang YL et al (2000) Impedance studies of oxygen exchange on dense thin film electrodes of $La_{0.5}Sr_{0.5}CoO_{3-\delta}$. J Electrochem Soc 147(11):4001–4007
126. Yang YL et al (2001) Oxygen exchange kinetics on a highly oriented $La_{0.5}Sr_{0.5}CoO_{3-\delta}$ thin film prepared by pulsed-laser deposition. Appl Phys Lett 79(6):776–778
127. Ringuedé A, Fouletier J (2001) Oxygen reaction on strontium-doped lanthanum cobaltite dense electrodes at intermediate temperatures. Solid State Ionics 139(3–4):167–177
128. Brichzin V et al (2002) The geometry dependence of the polarization resistance of Sr-doped $LaMnO_3$ microelectrodes on yttria-stabilized zirconia. Solid State Ionics 152–153:499–507
129. Kawada T et al (2002) Determination of oxygen vacancy concentration in a thin film of $La_{0.6}Sr_{0.4}CoO_{3-\delta}$ by an electrochemical method. J Electrochem Soc 149(7):E252–E259

130. Baumann FS et al (2005) Strong performance improvement of $La_{0.6}Sr_{0.4}Co_{0.8}Fe_{0.2}O_{3-\delta}$ SOFC cathodes by electrochemical activation. J Electrochem Soc 152(10):A2074–A2079
131. Koep E et al (2005) Characteristic thickness for a dense $La_{0.8}Sr_{0.2}MnO_3$ electrode. Electrochem Solid St 8(11):A592–A595
132. la O' GJ, Savinell RF, Shao-Horn Y (2009) Activity enhancement of dense strontium-doped lanthanum manganite thin films under cathodic polarization: a combined AES and XPS study. J Electrochem Soc 156(6):B771–B781
133. Januschewsky J et al (2009) Optimized $La_{0.6}Sr_{0.4}CoO_{3-\delta}$ thin-film electrodes with extremely fast oxygen-reduction kinetics. Adv Funct Mater 19(19):3151–3156
134. Ruiz de Larramendi I et al (2008) Structure and impedance spectroscopy of Pr_{1-x} Sr_x $Fe_{0.8}Co_{0.2}O_{3-\delta}$ (x=0.1, 0.2, 0.3) thin films grown by laser ablation. Appl Phys A Mater 93(3):655–661
135. Kawada T et al (1999) Oxygen isotope exchange with a dense $La_{0.6}Sr_{0.4}CoO_{3-\delta}$ electrode on a $Ce_{0.9}Ca_{0.1}O_{1.9}$ electrolyte. Solid State Ionics 121(1–4):271–279
136. Kim G et al (2007) Rapid oxygen ion diffusion and surface exchange kinetics in $PrBaCo_2O_{5+x}$ with a perovskite related structure and ordered a cations. J Mater Chem 17(24):2500–2505
137. Chen X et al (2002) Electrical conductivity relaxation studies of an epitaxial $La_{0.5}Sr_{0.5}CoO_{3-\delta}$ thin film. Solid State Ionics 146 (3–4):405–413
138. Fister TT et al (2008) In situ characterization of strontium surface segregation in epitaxial $La_{0.7}Sr_{0.3}MnO_3$ thin films as a function of oxygen partial pressure. Appl Phys Lett 93(15):151904
139. la O' GJ et al (2010) Catalytic activity enhancement for oxygen reduction on epitaxial perovskite thin films for solid-oxide fuel cells. Angew Chem Int Edit 49:5344–5347
140. Ruddlesden SN, Popper P (1958) Acta Crystallogr 11:54–55
141. Garcia G et al (2008) Electrical conductivity and oxygen exchange kinetics of $La_2NiO_{4+\delta}$ thin films grown by chemical vapor deposition. J Electrochem Soc 155(3):P28–P32
142. Burriel M et al (2008) Enhancing total conductivity of $La_2NiO_{4+\delta}$ epitaxial thin films by reducing thickness. J Phys Chem C 112 (29):10982–10987
143. Bassat JM, Odier P, Loup JP (1994) The semiconductor-to-metal transition in question in $La_{2-x}NiO_{4+\delta}$ (δ>0 or δ<0). J Solid State Chem 110(1):124–135
144. Burriel M et al (2007) Enhanced high-temperature electronic transport properties in nanostructured epitaxial thin films of the $La_{n+1}Ni_nO_{3n+1}$ Ruddlesden–Popper series (n=1, 2, 3, infinity). Chem Mater 19:4056–4062
145. Maignan A et al (1999) Structural and magnetic studies of ordered oxygen-deficient perovskites $LnBaCo_2O_{5+\delta}$, closely related to the "112" structure. J Solid State Chem 142(2):247–260
146. Kasper N (2008) Epitaxial growth and properties of (001)-oriented $TbBaCo_2O_{6-\delta}$ films. J Appl Phys 103(1):013907
147. Kim G et al (2006) Oxygen exchange kinetics of epitaxial $PrBaCo_2O_{5+\delta}$ thin films. Appl Phys Lett 88(2):024103
148. Yuan Z et al (2007) Epitaxial behavior and transport properties of $PrBaCo_2O_5$ thin films on (001) $SrTiO_3$. Appl Phys Lett 90 (21):21211
149. Liu J et al (2010) Epitaxial nature and transport properties in $(LaBa)Co_2O_{5+\delta}$ thin films. Chem Mater 22(3):799–802
150. Liu J et al (2010) PO_2 dependant resistance switch effect in highly epitaxial $(LaBa)Co_2O_{5+\delta}$ thin films. Appl Phys Lett 97 (9):094101
151. Grygiel C et al (2010) A-site order control in mixed conductor $NdBaCo_2O_{5+\delta}$ films through manipulation of growth kinetics. Chem Mater 22(6):1955–1957
152. Burriel M et al (2010) Influence of the microstructure on the high-temperature transport properties of $GdBaCo_2O_{5.5+\delta}$ epitaxial film. Chem Mater 22(19):5512–5520
153. Solis C et al (2008) Unusual strain accommodation and conductivity enhancement by structure modulation variations in $Sr_4Fe_6O_{12+\delta}$ epitaxial films. Adv Funct Mater 18(5):785–793
154. Fisher C, Islam M (2005) Mixed ionic/electronic conductors $Sr_2Fe_2O_5$ and $Sr_4Fe_6O_{13}$: atomic-scale studies of defects and ion migration. J Mater Chem 15(31):3200–3207
155. Putna ES et al (1995) Ceria-based anodes for the direct oxidation of methane in solid oxide fuel cells. Langmuir 11(12):4832–4837
156. Huang B et al (2010) Characterization of the Ni–ScSZ anode with a LSCM–CeO_2 catalyst layer in thin film solid oxide fuel cell running on ethanol fuel. J Power Sources 195(10):3053–3059
157. Huang H, Holme T, Prinz FB (2010) Increased cathodic kinetics on platinum in IT-SOFCs by inserting highly ionic-conducting nanocrystalline materials. J Fuel Cell Sci Tech 7(4):041012
158. Tucker MC (2010) Progress in metal-supported solid oxide fuel cells: a review. J Power Sources 195(15):4570–4582
159. Bieberle-Hütter A et al (2008) A micro-solid oxide fuel cell system as battery replacement. J Power Sources 177(1):123–130
160. Evans A et al (2009) Micro-solid oxide fuel cells: status, challenges, and chances. Monatsh Chem 140(9):975–983
161. Hertz JL, Tuller HL (2004) Electrochemical characterization of thin films for a micro-solid oxide fuel cell. J Electroceram 13 (1):663–668
162. Muecke UP et al (2008) Micro solid oxide fuel cells on glass ceramic substrates. Adv Funct Mater 18(20):3158–3168
163. O' GJL et al (2007) Recent advances in microdevices for electrochemical energy conversion and storage. Int J Energ Res 31(6–7):548–575
164. Chen M et al (2009) Preparation and electrochemical properties of Ni-SDC thin films for IT-SOFC anode. J Membrane Sci 334 (1–2):138–147
165. Ju YW et al (2010) Preparation of Ni–Fe bimetallic porous anode support for solid oxide fuel cells using $LaGaO_3$ based electrolyte film with high power density. J Power Sources 195(19):6294–6300
166. Lashtabeg A et al (2010) The effects of templating synthesis procedures on the microstructure of yttria stabilised zirconia (YSZ) and NiO/YSZ templated thin films. Ceram Int 36(2):653–659
167. Liu L, Kim GY, Chandra A (2010) Fabrication of solid oxide fuel cell anode electrode by spray pyrolysis. J Power Sources 195(20):7046–7053
168. Noh HS et al (2009) Physical and microstructural properties of NiO- and Ni-YSZ composite thin films fabricated by pulsed-laser deposition at T <700 degrees C. J Am Ceram Soc 92 (12):3059–3064
169. Rezugina E et al (2010) Ni–YSZ films deposited by reactive magnetron sputtering for SOFC applications. Surf Coat Tech 204 (15):2376–2380
170. Infortuna A et al (2009) Nanoporous Ni–$Ce_{0.8}Gd_{0.2}O_{1.9}$-thin film cermet SOFC anodes prepared by pulsed laser deposition. Phys Chem Chem Phys 11(19):3663–3670
171. Hertz J, Rothschild A, Tuller H (2009) Highly enhanced electrochemical performance of silicon-free platinum–yttria stabilized zirconia interfaces. J Electroceram 22(4):428–435
172. Choi S-H et al (2006) Fabrication and properties of porous Ni thin films. J Korean Ceram Soc 43(5):265–269
173. Brandner M et al (2008) Electrically conductive diffusion barrier layers for metal-supported SOFC. Solid State Ionics 179(27–32):1501–1504
174. Chen K et al (2008) Performance of an anode-supported SOFC with anode functional layers. Electrochim Acta 53(27):7825–7830

175. Cheng Z, Zha SW, Liu ML (2006) Stability of materials as candidates for sulfur-resistant anodes of solid oxide fuel cells. J Electrochem Soc 153(7):A1302–A1309
176. Fergus JW (2006) Oxide anode materials for solid oxide fuel cells. Solid State Ionics 177(17–18):1529–1541
177. Kolodiazhnyi T, Petric A (2005) The applicability of Sr-deficient *n*-type $SrTiO_3$ for SOFC anodes. J Electroceram 15 (1):5–11
178. Kurokawa H et al (2007) Y-doped $SrTiO_3$ based sulfur tolerant anode for solid oxide fuel cells. J Power Sources 164(2):510–518
179. Marina OA, Canfield NL, Stevenson JW (2002) Thermal, electrical, and electrocatalytical properties of lanthanum-doped strontium titanate. Solid State Ionics 149(1–2):21–28
180. Tao S, Irvine JTS (2003) A redox-stable efficient anode for solid-oxide fuel cells. Nat Mater 2(5):320–323
181. Tao S, Irvine JT (2004) Discovery and characterization of novel oxide anodes for solid oxide fuel cells. Chem Rec 4(2):83–95
182. Fleig J, Tuller HL, Maier J (2004) Electrodes and electrolytes in micro-SOFCs: a discussion of geometrical constraints. Solid State Ionics 174(1–4):261–270
183. Kuhn M et al (2008) Experimental study of current collection in single-chamber micro solid oxide fuel cells with comblike electrodes. J Electrochem Soc 155(10):B994–B1000
184. Tuller HL, Litzelman SJ, Jung W (2009) Micro-ionics: next generation power sources. Phys Chem Chem Phys 11(17):3023–3034
185. Frontera C et al (2002) Selective spin-state switch and metal–insulator transition in $GdBaCo_2O_{5.5}$. Phys Rev B 65(18):180405